Treating Energetics-contaminated Wastewater

by

Chenwei Zheng

A Thesis Presented in Partial Fulfillment
of the Requirements for the Degree
Master of Science

Approved October 2019 by the
Graduate Supervisory Committee:

Bruce E. Rittmann, Chair
Anca Delgado
Yenjung Sean Lai

ARIZONA STATE UNIVERSITY

December 2019

ABSTRACT

This study reports on the treatment of ammunition wastewater containing RDX (1,3,5-Trinitro-1,3,5-triazinane), HMX (1,3,5,7-Tetranitro-1,3,5,7-tetrazoctane), and the oxyanion co-contaminants nitrate (NO_3^-) and perchlorate (ClO_4^-) in a membrane biofilm reactor (MBfR), a Palladium (Pd)-coated MBfR (Pd-MBfR), and an abiotic Pd-coated film reactor (Pd-film reactor). A consortium of nitrate- and perchlorate-reducing bacteria, continuously fed with synesthetic ammunition wastewater featuring 4 mM nitrate and 0.1-2 mM perchlorate, formed robust biofilms on the membrane surfaces in the MBfR and Pd-MBfR. PdNPs with diameter 4-5-nm auto-assembled and stabilized on the surfaces of membrane and biofilm in MPfR and Pd-MBfR. Nitrate and perchlorate were rapidly reduced by the biofilms in the MBfR and Pd-MBfR, but they were not catalytically reduced through PdNPs alone in the MPfR. In contrast, RDX or HMX were recalcitrant to enzymatic degradation in MBfR, but was rapidly reduced through Pd-catalytic denitration in the MPfR and Pd-MBfR to form –N–NHOH or –N–H. Based on the experimental results, synergistic coupling of Pd-based catalysis and microbial activity in the Pd-MBfR should be a viable new technology for treating ammunition wastewater.

ACKNOWLEDGEMENT

I sincerely appreciate Dr. Bruce Rittmann, my advisor, for giving me instructions and providing me chance to be a part of Swette Center. This experience changed my future as it is the basic of my following steps. Thanks for Dr. Rittmann, I learnt more about Environmental Engineering like what is biofilm and microbiology, how important is mass balance. With his comments and advises in my progressive report, I learnt how to introduce my research as a story and improve my writing skills.

I appreciate Dr. Chen Zhou, my mentor, who is one of the best people I met in this country. He not only guided me in experiments and research, but also solved my puzzles in life. Most importantly, he behaved as an example, who know how to focus on what he likes. He knows how to grape the most important thing and ignore something negligible.

I owe thanks to Jianfang Wang, Yihao luo, Hua Xu, Min Long, Xiong Zheng, Yen-jung Lai, Steven, Michelle for their help on my research. I thank for Sarah and Carole who give me support. It's my honor to work with such an excellent group. I thank Dr. Anca Delgado serve as the committee members for my defense and gave me advises.

I would like to thank my families who love me, support me and be someone I love.

I could not imagine my past two years if I did not enter lab and do experiments. I may be the one who enjoy most of my time to play with friends. I may be the one who only focus on classes and stay at home for all my rest time. I may be the one who never know what research is and what experiments are. I may change another major. I may still have no destination. But I feel like the one who I am at present is the best one I can image.

TABLE OF CONTENTS

Page

Page

LIST OF FIGURES

Figure Page

Figure Page

LIST OF TABLES

INTRODUCTION

Ammunition wastewater, generated during manufacturing and decommissioning of munitions, contains metals, nitroaromatic compounds, and various oxyanions. Improper disposal of the ammunition wastewater leads to contamination of soil and groundwater, causing human- and environmental health concerns. Adequate treatment of the complex chemicals before discharge is imperative, and my project addresses a novel means to treat ammunition wastewaters.

1.1 Introduction to Ammunition Wastewater

Ammunition generally contains nitroaromatic compounds such as RDX (1,3,5-trinitro-1,3,5-triazacyclohexane) or HMX (1,3,5,6-tetranitro-1,3,5,7-tetrazocane) (Pennington & Brannon, 2002). These nitroaromatic energetics are widely used in a variety of munitions (Atikovic, Suidan, & Maloney, 2008). Due to its relative stability, RDX is the most common energetic used. For example, the famous Picatinny Arsenal Explosive 21 (PAX-21) is composed of RDX and 2,4-dinitroanisole (DNAN) (Ahn, Cha, Kim, & Oh, 2011). RDX is often combined with perchlorate (ClO_4^-) to lower the sensitives to the accidental explosion. Nitrate (NO_3^-) is another common co-contaminant (Oh, Cha, Chiu, & Kim, 2006) that has well-known human-health impacts.

The energetics are discharged to wastewater during the loading, assembling, and packing the munitions, along with steam washout for the disposal and deactivation of old munitions. The amounts are large. For example, the US. Department of Energy generates around 50,000 kg/year of RDX/HMX-containing wastewater as it dismantles nuclear weapons (Alnaizy & Akgerman, 1999). Improper disposal and inefficient

pretreatment then lead to severe contamination of groundwater and soil around the munition areas (Ahn et al., 2011). Due to their adverse effects on human health, ammunition wastewater featuring energetics, ClO_4^-, and NO_3^- require effective treatment before their discharge. The energetics generally are recalcitrant to biological treatment (Xiong, Yuan, Lai, Yang, & Zhou, 2016).

1.2 The Energetics

RDX, which stands for Royal Demolition Explosive, is a widely used energetic because it is stable in storage and is considered one of the most energetic of the military explosives (ExplosiVes, 1984). RDX has low volatility, with an air-water partition coefficient of $2x10^{-11}$ atm-m^3/mol, and high water solubility (35 mg/L water) (Terracciano et al., 2018), contributing to its presence in groundwater.

Being a nitramide, RDX has gotten a great deal of attention due to its adverse effects on the central nervous system (Etnier, 1989). The adverse effects of RDX and its transformation products apply to a wide range of organisms, including algae, fish, and humans (Van Aken, Yoon, & Schnoor, 2004). For example, the United States Environmental Protection Agency (EPA) has classified RDX as a group C carcinogen, which means that it is possibly carcinogenic to humans with limited animal evidence (EPA, 2014).

RDX has been introduced to soil and water around ammunition areas because of improper disposal of RDX-containing wastes. Ammunition wastewater generally contains 20-90 mg/L (90-405 μmol/L) RDX (Ahn et al., 2011; Jalal Hawari et al., 2000;

Oh et al., 2006). EPA risk assessments indicate that the drinking water concentration representing a 10^{-6} cancer risk level for RDX is 0.3 µg/L (0.001 µmol/L) (EPA, 2014). The EPA (2014) has listed the cyclic nitramine RDX as a priority pollutant.

RDX also is notorious for being recalcitrant to biodegradation (Xiong et al., 2016). Although RDX is biodegradable by *Gammaproteobacteria* in anaerobic conditions (Cupples, 2013), the conventional biological treatment processes are not sufficient to mineralize the nitroaromatic compounds, because the nitro constituents in energetics inhibit the enzyme-catalyzed electrophilic attack (Clark & Boopathy, 2007). Furthermore, anaerobic biodegradation can produce equal or more toxic products, such as azoxy and azo-compounds (Jalal Hawari et al., 1999). The toxic products and slow rate have made biotransformation unpractical for large scale RDX treatment.

HMX is a more complex cyclic nitroamide contaminant in ammunition wastewater, compared to RDX (Heilmann, Wiesmann, & Stenstrom, 1996). It has gradually replaced its homolog RDX in importance because of its resistance to unwanted denotation. HMX explodes at the temperature of 534°F (279°C), and the military uses it in certain applications, including nuclear devices, plastic explosives, rocket fuels, and booster charges (DSS, 2015). HMX dissolves slightly in water, which leads to HMX-contaminated groundwater near munition sites.

The Delaware Health and Social Services (DSS) report that studies on animals indicate HMX has adverse effects on the nervous system and liver (DSS, 2015). HMX will cause a breakdown of the circulatory system and a central nervous system

disturbance with intravenous injection (Cao & Li, 2018). HMX can cause cardiovascular depression or atrophy, resulting in hyperactivity and convulsions (Y. Chen et al., 2011).

People can be exposed to HMX by drinking HMX-contaminated water. The contamination occurs in the groundwater near places where HMX was used or made, including ammunition-wastewater treatment plants. Ammunition wastewater generally contains 4 – 170 mg/L (130 – 570 μmol/L) HMX (Cao & Li, 2018; Morley, Henke, & Speitel Jr, 2005). Unwanted leaks or improper disposal introduce HMX to the groundwater. Due to its adverse effects on mammals, EPA recommends that the concentration of HMX in an adult's drinking water be less than 0.4 mg/L.

HMX is an explosive that is very much like RDX in its structure, and this makes it generally recalcitrant to biodegradation, although it can be biodegraded. *Methylobacterium* (Fournier, Trott, Hawari, & Spain, 2005), *Morganella morganii* (Kitts, Cunningham, & Unkefer, 1994), *Citrobacter freundii* (J-S Zhao, Paquet, Halasz, & Hawari, 2003), *Clostridium sp.* (Jian-Shen Zhao, Greer, Thiboutot, Ampleman, & Hawari, 2004; Jian-Shen Zhao, Paquet, Halasz, Manno, & Hawari, 2004; Jian-Shen Zhao, Spain, & Hawari, 2003), *Methylobacterium* (Van Aken et al., 2004) and denitrifying bacteria *Pseudomonas* and *Bacillus* (Singh, Soni, Kumar, Purohit, & Singh, 2009) were tested and confirmed to able to degrade HMX.

Studies also were conducted with a mixed culture enriched from anaerobic digester sludge (Boopathy, 2001). The fastest HMX removal (from 20 mg/L to 0.05 mg/L) needed more than 10 days in anaerobic conditions with a mixture of electron acceptors. No biodegradation was observed in aerobic conditions (Boopathy, 2001). Although slow

kinetics and toxic byproducts are the main problems for biodegradation of HMX, biodegradation remains a potentially cost-effective and environmentally friendly treatment.

1.3 The Oxyanions

The energetics usually occur in mixtures with oxyanions ClO_4^- and NO_3^- in ammunition wastewater. ClO_4^- in the form of ammonium perchlorate ($NH_4ClO_4^-$) is widely used as an oxidant and energetics booster in solid propellants for rockets, missiles, and fireworks (EPA, 2017). Ammonium perchlorate is highly soluble in water, ~ 200 g/L. Because of its low vapor pressure, perchlorate ions do not volatilize from water or soil surfaces to air. Perchlorate is relatively stable and mobile in water, contributing to its extensive existence in the aqueous system.

The primary pathways for human exposure to ClO_4^- are ingestion of contaminated food and drinking water (EPA, 2017). ClO_4^- is known to have adverse effects on the thyroid gland and its hormones secretion by interfering with the uptake of iodide (National Research Council 2005). Perchlorate causes functional disruption of the thyroid and potentially leads to a reduction in the production of thyroid hormones, especially in infants and young children.

In a munition plant, ammonium perchlorate is combined with RDX to produce less-sensitive explosives. For example, ammonium perchlorate is one of the primary components of Picatinny Arsenal Explosive 21 (PAX-21) (Ahn et al., 2011). During the

manufacturing of ammunition like propellants and explosives, ClO_4^- is transferred to the wastewater in the ammunition plant. Ammunition wastewater can contain about 190 mg/L (~ 2 mmol/L) ClO_4^- (Ahn et al., 2011; Ahn, Hubbard, Cha, & Kim, 2014). The EPA has established an official reference Drinking Water Health Advisory of 15 µg/L and a tap-water screening level of 14 µg/L for perchlorate and its salts (EPA, 2017).

NO_3^- is commonly found as a co-contaminant in water with ClO_4^- in ammunition wastewater, because ammonium nitrate ($NH_4NO_3^-$) is a main component in explosives (EPA, 2014). NO_3^- is naturally occurring, making up a part of the nitrogen cycle (EPA, 1985). NO_3^- salts are highly soluble in water at standard temperature and pressure, leading to its ready transport through the soil and groundwater.

NO_3^- is a public-health risk for causing cancer and methemoglobinemia in infants below the age of six months (blue baby syndrome) (Kross, Ayebo, & Fuortes, 1992). EPA's maximum contaminant level (MCL) for NO_3^- is 10 mgN/L to protect against blue-baby syndrome. The World Health Organization has given an admission level for many industrial or human uses as less than 50 mg/L NO_3^-, which is approximately 11 mgN/L (Prüsse, Hähnlein, Daum, & Vorlop, 2000; Strukul et al., 2000).

The main methods of RDX manufacturing, the Woolwich and Bachmann processes, generate nitrate-containing ammunition wastewater (An, He, Huang, & Yang, 2010). The concentration of NO_3^- can be 2 to 5 orders of magnitude higher than the ClO_4^- concentration (Schaefer, Fuller, Condee, Lowey, & Hatzinger, 2007; H.-P. Zhao et al., 2011). Ammunition wastewater contains about 110 mg/L NO_3^- (~ 2 mmol/L) (Ahn et al., 2011; Ahn et al., 2014). Considering NO_3^- when treating ammunition wastewater is

critical, because NO_3^- may inhibit the reduction of ClO_4^- and cyclic nitramine explosives (An et al., 2010).

In general, ClO_4^- and NO_3^- co-contaminants can be removed via four main methods: ion exchange, membrane filtration, catalytic reduction, and microbial reduction. Ion exchange and membrane filtration (reverse osmosis) generate a concentrated brine that is difficult to dispose of. Catalytic and microbial reductions show great potential, but need to have improved treatment efficiency.

1.4 Existing Approaches to Treating Ammunition Wastewater

Multiple physical, chemical, and biological techniques have been applied for the treatment of ammunition wastewater, including adsorption using activated carbon (Morley, Speitel, & Fatemi, 2006), alkaline hydrolysis (Heilmann et al., 1996; Morley et al., 2005), photocatalysis (Y. Chen et al., 2011; Z. Liu, He, Li, & Liu, 2006; Pouretedal, Keshavarz, Yosefi, Shokrollahi, & Zali, 2009), photoelectrocatalysis (Tian, Hitchman, & Shamlian, 2012), electrochemical oxidation (Dai Lam, Van Chat, Bach, Loi, & Van Anh, 2014), Fenton oxidation (Anotai, Tanvanit, Garcia-Segura, & Lu, 2017; Cao & Li, 2018; Li, Hsieh, Mahmudov, Wei, & Huang, 2013), zero-valent iron (ZVI) reduction (Ahn et al., 2011; Ahn et al., 2014; Oh et al., 2006), Palladium (Pd) catalyzed reduction (Rahaim & Maleczka, 2005), microbial reduction (An et al., 2010; Atikovic et al., 2008; Cupples,

2013; Fuller, Hatzinger, Condee, & Togna, 2007), and phytoremediation by Vetiver glass (Panja, Sarkar, & Datta, 2018).

Adsorption using granular activated carbon (GAC) has been applied frequently in ammunition wastewater separation and treatment (Morley et al., 2006). GAC offers the advantages of having a large surface area that can adsorb perchlorate and the energetic compounds. However, treatment with GAC is expensive and also produces explosive-laden spent carbon, which possibly leads to the secondary contamination problems. The explosive-laden carbon cannot be thermally regenerated, because of the risk of explosion. GAC is not able to adsorb NO_3^- without other enhancement.

Alkaline hydrolysis is an alternative to the thermal regeneration of explosives-laden GAC (Heilmann et al., 1996). Complete hydrolysis of 36 mg/L RDX occurred in 15 minutes at 80℃, yielding nitrite and formate. A temperature decrease from 80℃ to 50℃ resulted in a significant decrease of removal rate so that less than 10% of 36 mg/L RDX was removed in 60 minutes (Heilmann et al., 1996). Using alkaline hydrolysis to treat wastewater directly from the ammunition plant is not economical due to the high-temperature requirement.

Photocatalysis under simulated sunlight with nano-sized titanium dioxide (nano-TiO_2) loaded onto an active carbon fiber (ACF) cloth showed efficient degradation of the energetics (Z. Liu et al., 2006). The formation of hydroxyl radicals (·OH) was involved in the decomposition of the energetics. First-order reaction kinetics described energetics degradation. 20 mg/L RDX was 99.9% removed in 120 minutes by NanoTiO_2-based

photocatalysis in the first run, but the efficiency of the catalyst drastically decreased with repeated uses, making it unpractical for ammunition wastewater (Z. Liu et al., 2006).

Fenton's reaction, a well-known form of advanced oxidation, has shown promise for treating energetics-contaminated wastewater. The energetics could be mineralized by non-selective OH-radicals generated during the Fenton reaction, which involves the decomposition of H_2O_2 using a Fe catalyst (Anotai et al., 2017). Conventional Fenton reagents were reported to remove 20 mg/L RDX in 180 minutes (Dai Lam et al., 2014). Several strategies have been studied to enhance the Fenton's process. For instance, electrochemical oxidation with Fenton's process needed 120 minutes to remove 175 mg/L RDX, while electro-assisted Fenton's process was able to remove the same amount of RDX in 60 minutes (Anotai et al., 2017). Although the electro-assisted Fenton's process shows potential in energetics removal, the data reported by Anotai et al. (2017) indicate that DOC removal was insignificant during the 120 minutes, which means that the energetics were not mineralized.

Palladium-catalyzed hydrogenation of energetics was first reported by EwenáSmith (2002). The hydrogenation by H_2 and Pd coated on carbon gave unstable intermediates that rearranged to hexamethylenetetramine. However, little information documented the mechanisms or pathways. Since Pd was reported not catalyze the NO_3^- reduction, this method may not be applicable when oxyanions are co-contaminants.

Biological reduction is one of the most studied methods for treating energetics-containing wastewater, and it can be a cost-effective technology to treat ammunition wastewater (An et al., 2010). Biological reduction of perchlorate has been studied for

over 20 years. The bacteria use perchlorate as an electron acceptor for their metabolism (Luo et al., 2015; Ontiveros-Valencia, Tang, Krajmalnik-Brown, & Rittmann, 2014). *Dechlorospirillum* and *Dechlomonas* of the class *Beta-Proteobacteria* are the main genera of perchlorate-reducing strains (PRSs) (Ye, You, Yao, & Su, 2012).

For energetics, McCormick, Cornell, and Kaplan (1981) reported that RDX was biodegradable and postulated that RDX was reduced to hexahydro-1-nitroso-3,5-dinitro-1,3,5-triazine (MNX), hexahydro-1,3-dinitro-5-nitro-1,3,5-triazine (DNX), and hexahydro-1,3,5-trinitroso-1,3,5-triazine (TNX) in anaerobic conditions. The *Gammaproteobacteria* class contains the majority of known energetics-degrading isolates (Cupples, 2013). The energetics also can be mineralized in aerobic conditions by several strains of bacteria, including *Stenotrophomonas maltophilia*, *Rhodococcus* sp. strain A, and *Rhodococcus* sp. strain D22 (J Hawari, Beaudet, Halasz, Thiboutot, & Ampleman, 2000). Cyclic nitramine ring-cleavage and N_2O generation occur during the aerobic mineralization. Although biodegradation is a promising method to mineralize energetics, complete removal of 31 mg/L RDX in anaerobic conditions needed 12 days (An et al., 2010). If a biological process requires a long time to completely remove RDX or HMX, it may be unpractical for large-scale treatment.

Microbial reduction combined with zero-valent iron (ZVI) reduction was reported to be an efficient method to biodegrade ClO_4^- and energetics found together in wastewater (Ahn et al., 2014). ZVI granules could transform the recalcitrant energetics to ring-cleavage products, which could be utilized as the electron donor for perchlorate reducing bacteria (PRB) that continuously consumed ClO_4^- as electron acceptor (Ahn et al., 2014).

In this study, ~50 mg/L RDX was completely reduced to formaldehyde in 120 minutes. However, 100% removal of 120 mg/L ClO_4^- needed 5 days.

Phytoremediation using vetiver grass (*Chrysopogon zizanioides*) was effective in removing explosive compounds from ammunition wastewater. Vetiver grass has been widely used in the remediation of contaminated soil and water. It has a massive, dense root system, grows fast, and can tolerate the stress imposed by the explosives (Panja et al., 2018). Although phytoremediation is environmentally friendly, it has a prolonged removal rate: e.g., 20 days were needed for the degradation of 12 mg/L RDX.

1.5 Pd-MBfR: A Promising Technology for Removing Co-contaminants in Ammunition Wastewater

Most of the technologies noted above do not lead to the complete break-down of cyclic nitramines. They also have limitations of high cost or slow removal rates. To address these problems, I developed a novel synergetic platform for cost-effective co-contaminant reduction of RDX, HMX, ClO_4^- and NO_3^-; it is based on palladium-catalyzed reduction plus biodegradation.

Palladium can catalyze NO_2^- reduction (Shin, Jung, Bae, Lee, & Kim, 2014; Zhou et al., 2017a) in the presence of H_2. Pd has exceptional H_2 adsorption capability (900-fold of its volume). The H_2 adsorbed on the surface can be transferred to the oxygen atoms of oxyanions, which are at lower redox states than Pd, forming H_2O. The N selectivity to N_2 or NH_4^+ is a key regarding Pd catalyzed NO_2^- reductions. Pd alone can also catalyze

the hydroxygenation of oxyanions ion the presence of H_2, such as for ClO_3^- (B. P. Chaplin et al., 2012; J. Liu et al., 2014), whereas NO_3^- and ClO_4^- require a secondary "promoter" metal (Cu, Sn, and In) (B. P. Chaplin et al., 2012).

Palladium can catalyze denitration and hydrogenation of nitramines (B. P. Chaplin et al., 2012; EwenáSmith, 2002; Ranea, Strathmann, Shapley, & Schneider, 2011). In the study of EwenáSmith, the first study that controlled the RDX reduction, Pd coated on C or NaBH showed potential to reduce N-nitrosodimethylamine, generating hexamethylenetetramine, which was identified by Proton Nuclear Magnetci Resonance (HNMR). Based on the products detected, RDX was proposed to be denitrated from nitramines to hydrazine, which was then rearranged to hexamethylenetetramine. The study did not provide detailed kinetics or mechanisms of Pd-catalyzed RDX reductions, but other studies reported in more detail the decomposition of N-nitrosodimethylamine to aromatic-NH_2 products (Ranea et al., 2011) or aromatic-NHOH products (Rahaim & Maleczka, 2005). The kinetics and mechanisms of RDX degradation catalyzed by Pd have received very little study, and existing research does not identify the products of Pd-catalyzed reduction of RDX or the efficiency of Pd catalysts.

Since Pd alone cannot catalyze ClO_4^- or NO_3^- reductions, the keys to success are co-immbolization of PdNPs and biofilm on gas-transfer membranes that deliver the electron donor for each reduction reaction, H_2 gas. Membrane biofilm reactor (MBfR), first devised by Rittmann et al. (2004), is a platform delivering H_2, providing large surface area for biofilm and catalysts, and being able to continuously treat water. In an MBfR fed NO_3^- and ClO_4^-, the oxyanions are reduced by an autotrophic biofilm consisting of

denitrifying bacteria and perchlorate-reducing bacteria that naturally develop on the outside of the membrane. The H_2 delivered via the hollow fiber membrane serves as the electron donor, while NO_3^- or ClO_4^- are the electron acceptors. The carbon source, CO_2, is supplied to the reactor via mixed CO_2-H_2 gas or as bicarbonate in the medium. Nitrate and perchlorate removal fluxes can reach as high as 5.4 $gNm^{-2}d^{-1}$ and 5.0 $gClO_4m^{-2}d^{-1}$, corresponding to 2000 mEq $m^{-2}d^{-1}$ for N and 200 mEq $m^{-2}d^{-1}$ for ClO_4^- (Van Ginkel et al., 2008).

Efficient H_2 supply is provided using nonporous hollow-fiber membranes, which also are the substrata for biofilms associated that produce auto-assembled palladium nanoparticles (PdNPs) (Zhou et al., 2016; Zhou et al., 2017a). The concept is an extension of the H_2-based membrane biofilm reactor (MBfR), in which biofilms are associated with the membrane giving a sufficient H_2 supply. When PdNPs are co-immobilized with the biofilm, the process becomes the Pd-MBfR. The Pd-MBfR provides a highly efficiently supply H_2 to the biofilm and PdNPs. The simultaneous microbially driven and Pd-catalyzed NO_3^- reduction was evaluated by Zhou et al. (2017a), who documented that carefully controlled delivery of H_2 enabled accurate control of N selectivity to attenuate unwanted NH_4^+ formation. NO_3^- is reduced to harmless N_2 via bioreduction plus PdNPs-catalysis (Zhou et al., 2017a). The energetics are catalytically reduced to products that eventually ought to be biodegradable. A detailed description of the Pd-MBfR is in the section “Experimental reactor set up.”

1.6. Overview of the Thesis

Chapter 2 introduces the experimental methods, Chapter 3 summarizes oxyanions treatment in three reactors, and Chapter 4 summarizes energetics treatment in the three reactors. Chapter 5 provides conclusions and recommended future work.

MATERIALS AND METHODS

2.1 Reactor Setup and Experimental Methods

Three identical bench-scale reactors included dual glass tubes connected by a small sealed bottle for gas sampling, as illustrated in Fig 2.1. Each reactor, having a total working volume of 75 ml, contained a main bundle with 50 hollow-fiber membranes (composite bubble-less gas – transfer membrane, 280 μm OD, 180 μm ID, wall thickness 50 μm; Model MHF 200TL Mitsubishi Rayon Co., Ltd, Tokyo, Japan) and a "coupon" bundle with 10 same composite fibers in two glass tube, respectively. Each fiber was 18-cm long, giving a total membrane surface of 92.4 cm^2. Premixed gas (80%-H_2/20%-CO_2) was supplied to all the ends of fiber bundles at different pressures controlled by a pressure regulator. A solute's concentration inside a reactor was equal to its effluent concentration due to mixing by a recirculating pump with a rate of 150 ml/min.

The glass bottle contained 15 ml liquid volume and about 30 ml gas volume that enabled sampling and measurement of gaseous products, such as N_2 and N_2O. Liquid samples were collected from the liquid sample point in Figure 2.1 using a 5-ml syringe and immediately filtered through 0.2-μm pore-size syringe filter (PGVDF membrane, GE Healthcare Life Sciences Whatman^{TM}) into 2-ml glass vials for ion chromatography tests and storage.

The three reactors, one H_2-based abiotic reactor and two membrane biofilm reactors (MBfR), were operated in batch and continuous modes at room temperature (~ 25°C) to investigate the efficiency of reducing NO_3^-, ClO_4^-, RDX, and the common co-contaminants -- NO_2^- and ClO_3^-.

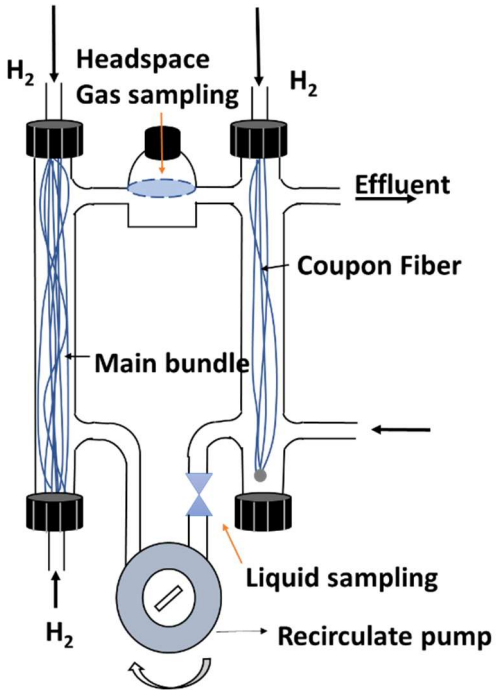

Figure 2.1. Schematic Diagram of the Reactor System.

To carry out abiotic tests, Pd was coated on the membrane in one reactor by introducing 2 mM of anaerobic Na_2PdCl_4 solution to the reactor. The temperature was 25°C, and the medium pH was ~9 set with 14 mM phosphate buffer. Pd^{2+} was reduced to Pd° that was immobilized on the membranes. Reduction corresponded to the brown Na_2PdCl_4 solution turning to black as Pd^{2+}, but the solution became clear as Pd° formed on the membrane surfaces. The reduction and coating process lasted 12 hours for composite membranes, as shown in Figure 2.2, creating a membrane palladium-film reactor, or MPfR.

Figure 2.2. Pictures of Pd^{2+} Reduction and Pd^{0} Immobilization.

To compare Pd with other metal catalysts, I set up two other abiotic reactors: Re-MPfR and Rh reactor. For the Rh reactor, Rh was coated on the membrane in one reactor by introducing 2 mM of anaerobic Rh solution to the reactor, following the same pattern of MPfR.

For Re-Pd bimetallic catalyst synthesis, I introduced the Re solution to the Pd-coated composite membranes reactor, creating Re-Pd coated MBfR, or Re-MPfR. The pH value gradually increased, probably due to the reaction:

$$ReO_4^- + H_2 + H^+ \rightarrow 0.5Re_2O_5(s) + 1.5H_2O$$

The pH became stable at 5.3 after 2 hours, suggesting that the proton-consuming reaction was completed and the reactor was a Re-MPfR. Assuming that all the Re was immobilized on the Pd layer, the new Re-Pd layer featured a Re-to-Pd mole ratio of 1:2.

Two membranes were evaluated in separate tests: 1) a composite bubble-less gas-transfer membrane, 280 μm OD, 180 μm ID, wall thickness 50 μm; Model MHF 200TL Mitsubishi Rayon Co., Ltd, Tokyo, Japan, and 2) a nonporous polypropylene fiber, 200

μm OD, 100–110 μm ID, wall thickness 50–55 μm; Teijin, Ltd., Japan. The wall of the composite fiber has three layers: outer and inner layer are hydrophobic polyethylene layer with small pores of 0.1–0.15 μm, and the layer between the two outer layers is non-porous polyurethane of 1-μm thickness. The polypropylene hollow fibers are single-layer and non-porous (Tang et al., 2012).

H_2 permeation through the polymer membranes is controlled by diffusion, which follows Fick's first law at a steady-state (Tang et al., 2012). The driving force is the difference between the actual H_2 concentration in the liquid and the concentration of H_2 that would be in equilibrium with the H_2 pressure in the fiber lumen. The gas diffuses across the membrane without forming bubbles. In the MPfR, H_2 absorbed to the Pd catalyst formed on the membrane, generating atomic hydrogen (Zhou et al., 2017a).

To provide quantitative data to evaluate the performance of reactors, I calculated the maximum H_2 delivery flux of the electron defined according to Tang et al. (2012):

$$H_2\ max\ = \frac{k_2}{RT}\frac{D_{m,apparent}(P_0 - 1)}{Z_m}$$

$H_2 max$: maximum H_2 deliver capacity ($\frac{\mathrm{e^-equiv}}{\mathrm{m^2\ d}}$)

P_0: H_2 pressure in the hollow- fiber lumen (atm)

z_m: membrane thickness (m) (50 μm for composite membrane, 55 μm for polypropylene membrane

$D_{m,apparent}$: apparent H_2- diffusion coefficient in the membrane $\left(\frac{\mathrm{m^2}}{\mathrm{d}}\right)$

k_2: coefficient that converts H_2 from amount to equivalent $(\frac{2e^-}{mol})$

R: gas constant 0.082 $\left(\frac{L\ atm}{mol\ K}\right)$

T: Temperature (approximately 298.15 K)

I calculated the surface loading of the electron defined according to Zhou et al. (2016):

$$J_s = \frac{S_0 Q}{A}$$

J_s: Surface loading $(\frac{e^- mequiv}{m^2\ d})$

S_0: Influent total electron acceptor concentration $(\frac{e^- mequiv}{L})$

Q: Influent flow rate to the MBfR system (L/d)

A: Membrane surface area (m^2)

$D_{m,apparent}$ for the composite membrane and polypropylene membrane are 1.4×10^{-6} and 1.4×10^{-7} m^2/d, respectively (Tang et al., 2012). The polypropylene hollow fiber has a lower H_2 flux when applying the same gas pressure.

To explore catalytic reduction with Pd-based bimetal catalysts, I set up four bimetallic catalysts reactors (M-MPfR) -- Pt-MPfR, Ru-MPfR, Rh-MPfR, and Au-MPfR

-- and one Pd-film reactor as control. I coated 39 mg Pd on the composite membrane by introducing 75-mL 5-mM Pd solution to the five reactors following the same procedure of the Pd-film reactor, respectively. Then I introduced 75-ml 1-mM Pt solution to one of the reactors to create Pt-MPfR. Ru-MPfR, Rh-MPfR, Au-MPfR, and Pd-film reactor were created in the same way expect using different metal solutions. For bimetallic catalysts reactors, the ratio between Pd and the secondary metal is 5-mol: 1-mol.

For the biotic reactor, I set up in parallel two identical bench-scale MBfRs. I inoculated the two MBfRs with anoxic sludge from Mesa Northwest Wastewater Reclamation Plant (Mesa, AZ, USA) and continuously fed them for one month at a constant HRT of 20 hours with synthetic groundwater medium containing 4 mM NO_3^- and 0.1 mM ClO_4^- which are similar to the common groundwater contaminated by NO_3^- and ClO_4^- (Parker, Seyfferth, & Reese, 2008). After three months, thick, mature biofilms had formed on the fiber surfaces in both MBfRs.

Once the biofilms were mature, I introduced 2 mM Na_2PdCl_4 into one of the reactors. Within 1-day, Pd was immobilized as black precipitates in the biofilm matrix in the reactor, which is then named "Pd-MBfR." The other one with intact biofilm is then named "MBfR" (Fig. 2.3).

The MBfR and Pd-MBfR were operated in a continuous-flow mode at room temperature (~25°C) according to the series of conditions shown in Table 2-1. The synthetic groundwater was supplied to two reactors at the first 5 stages, and the synthetic ammunition wastewater (without energetics) was supplied in the last stage, designed to find the operational conditions that allowed removing both oxyanions and energetics.

Table 2-1. Operating Conditions for the Six Steady States Tested with the MBfR and Pd-MBfR Fed the Oxyanions

Steady state	Flow rate (Q) ml/min		HRT h		NO_3^- surface loading mEq/m^2-day		ClO_4^- surface loading mEq/m^2-day	
(SS)	MBfR	Pd-MBfR	MBfR	Pd-MBfR	MBfR	Pd-MBfR	MBfR	Pd-MBfR
SS1	0.08	0.08	12	14	240	240	10	7
SS2	0.17	0.18	7	7	550	550	24	24
SS3	0.21	0.21	6	6	740	740	31	42
SS4	0.30	0.28	4	4	950	830	43	37
SS5	0.31	0.29	4	4	906	860	39	39
SS6	0.30	0.30	4	4	910	870	810	830

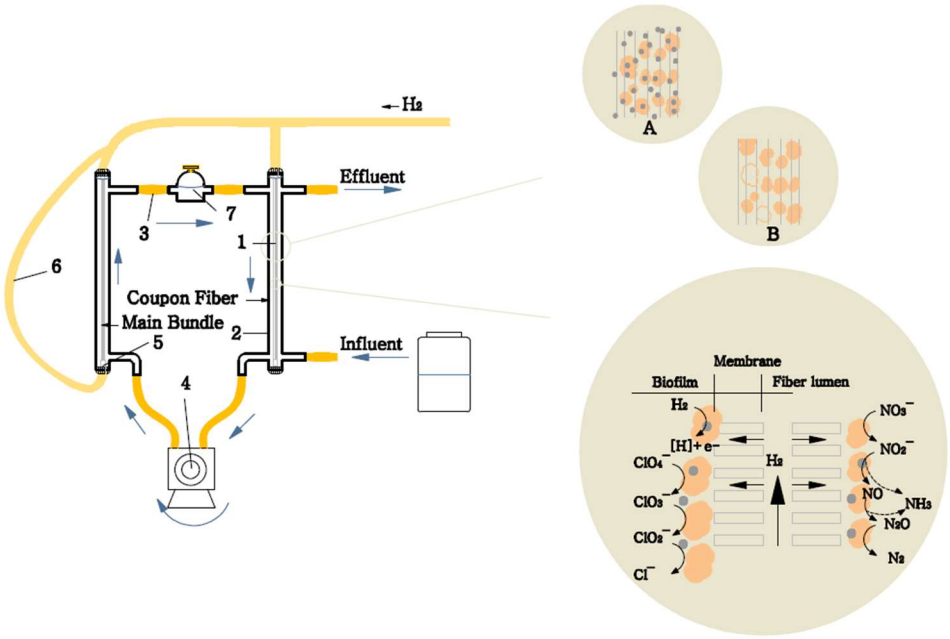

Figure 2.3. Schematic Diagram of the Reactor System (left) and of NO_3^- and ClO_4^- Reduction Pathways (right). A: Pd-MBfR, B: MBfR. Reactor system is composed of membrane bundles (1), two glass tube with 6 mm internal diameter and 27 cm length (2), propylene tube for liquid (3), recirculate pump (4), propylene tube for hydrogen gas (5) 15-ml liquid volume and 30-ml gas volume glass bottle (6).

After the reactors reached steady-state, batch tests for each oxyanions contaminant were conducted in the reactors to compare the reduction rates. Energetics were only tested at the end of stage 6 in several biotic and abiotic reactors in batch mode. The testing procedures are the same as NO_2^- tests in MPfR.

2.2 Chemical Analyses

RDX and HMX concentrations were measured using ultra-performance liquid chromatography (UPLC, Waters, Milford, MA, USA) with an ACQUITY UPLC column of 2.1 × 50 mm, and 1.7 μm BEH C_{18}. The mobile phase was an acetonitrile-in-water gradient from 10 to 30% at a flow rate of 0.3 ml/min. NO_3^-, NO_2^-, ClO_3^-, and Cl^- were measured using ion chromatography (Dionex ICS 3000) with an AS18 column and AG18 pre-column, an eluent concentration of 22 mM KOH, and 1-ml/min flow rate. ClO_4^- was measured using ion chromatography (Dionex ICS 3000) with an AS16 column and AG16 precolumn, an eluent concentration of 50 mM KOH, and 1-ml/min flow rate. N_2O and N_2 collected from the little bottle were assayed by Gas Chromatography. NH_4^+ was measured by HACH ammonia kit 830 with a range of 0.015-2 mg/L. The pH was measured with a pH probe (Thermo Electron Corporation).

Analysis of the reduction products of RDX or HMX was determined using a reversed-phase HPLC connected to a photodiode array (PDA) detector coupled with a Micromass benchtop single quadrupole mass detector. The samples were injected into a 3μm-pore size Hypersil Gold aQ column (50 x 2.1 mm i.d.) at 10 ℃. The solvent system

was composed of 20% acetonitrile:80% water (v/v). The electron-withdrawing nature of the hydrogen and sodium makes these molecules vulnerable to adduct formation with the mobile phase. The mass spectrometer was operated in the both positive- and negative-ion mode with Electrospray ionization (ESI). The desolvation gas flow was set to 600 L/h with a desolvation (dissociate electro-statically bound particles in an aqueous solution) temperature of 380 ℃. The cone gas flow was 80 L/h. The source temperature was set to 110 ℃. For mass analysis in this study, ionization was performed in a positive electrospray ionization mode, ES(+), producing mainly the deprotonated molecular mass ion [M+H].

2.3 Media Preparation

Synthetic groundwater medium: 1700 mg $NaNO_3$, 61 mg $NaClO_4$, 4970 mg Na_2HPO_4, 4200 mg NaH_2PO_4, 8.3 mg $Ca(NO_3)_2$, 7.4 mg $Mg(NO_3)_2$, and 5 ml trace metal solution were mixed in 5 L DI water.

Synthetic ammunition wastewater medium: 1700 mg $NaNO_3$, 1224 mg $NaClO_4$, 4970 mg Na_2HPO_4, 4200 mg NaH_2PO_4, 8.3 mg $Ca(NO_3)_2$, 7.4 mg $Mg(NO_3)_2$, and 5 ml trace metal solution were mixed in 5 L deionized (DI) water.

Trace metals solution: 100 mg $ZnSO_4 \cdot 7H_2O$, 30 mg $MnCl_2 \cdot 4H_2O$, 300 mg H_3BO_3, 200 mg $CoCl_2 \cdot 6H_2O$, 10 mg $CuCl_2 \cdot 2H_2O$, 10 mg $NiCl_2 \cdot 6H_2O$, and 30 mg Na_2SeO_3 were mixed in 1 L DI water (Wu et al., 2017).

Pd solution: Na_2PdCl_4 was used to prepare the Pd solution. 0.46 g Na_3PO_4 and 0.08 g NaH_2PO_4 were dissolved in 1 L DI water to get buffer with a pH value of 12. Then 2-mM Na_2PdCl_4 was added dropwise into the buffer. The liquid was aerated with N_2 gas to maintain anaerobic conditions. The Pd^{2+} solution was brown and free of turbidity.

Re solution: Rhenium oxide (Re_2O_7) was used to prepare the Re solution. 484 mg Re_2O_7 was dissolved in 1-L Deionized water to form 1 mM perrhenic acid ($HReO_4$) solution at an initial pH of 0. Then NaOH was added to increase the pH to 3.

Rh solution: Rhodium chloride hydrate ($RhCl_3 \cdot xH_2O$) was used to prepare the Rh solution. 0.46 g Na_3PO_4 and 0.08 g NaH_2PO_4 were dissolved in 1 L DI water to get buffer with a pH value of 12. Then 0.42 g $RhCl_3 \cdot xH_2O$ was added dropwise into the buffer. The liquid was aerated with N_2 gas to maintain anaerobic conditions. The Rh^{2+} solution was dark brown and free of turbidity.

RDX/HMX solution: A RDX + HMX solution (1000 mg/ml each in acetonitrile) was purchased from *SIGMA-ALDRICH*. 1-ml solution was diluted in 49-ml DI water to get a 20 mg/L RDX/HMX medium.

2.4 Biofilm Sampling and Analyses

I sampled the biofilm for the two MBfRs at the end of stage 1, which had a total electron-acceptor surface loading of 250 mEq/m^2-day; stage 4, which had a surface loading of 1000 mEq/m^2-day; stage 5, which had surface loading of 1000 mEq/m^2-day and more Pd coated on the biofilm in Pd-MBfR; and stage 6, which had a surface loading

of 1700 mEq/m^2-day. Biofilm samples were taken from fibers using sterilized tweezers and then placed into a 2-ml centrifuge tube with 1.0 ml DNA-free water, vortexed the tube for 15 min at the 8000 rpm (5900 × g) (Eppendorf 5415R, Eppendorf, Germany) at 4°C. The supernatant was carefully decanted. The pellets formed in the centrifuges were moved into PowerBead tubes for downstream DNA extraction using the DNeasy Blood & Tissue Kit (QIAGEN, USA) and followed the manufacturer's recommendations. I quantified the DNA with a spectrophotometer (NanoDrop ND-1000, NanoDrop Technologies, USA) and documented its yield and purity based on the 260/280 nm absorbance ratio (Tataurov, You, & Owczarzy, 2008). Samples were stored at -80°C until qPCR and pyrosequencing analyses. Library preparation and sequencing were performed at the ASU Genomics Core in Center for Fundamental and Applied Microbiomics (https://biodesign.asu.edu/cfam). Amplicon sequencing of the V4 region of the 16S rRNA genes in all DNA samples was performed using the barcoded primer set 515F/806R (Caporaso et al., 2012). Raw sequences were processed using the QIIME 2.0 suite (Caporaso et al., 2010), as described in detail in Ontiveros-Valencia et al. (2014).

3.1 Oxyanion Reduction Tests: PdNPs as A Monometallic Catalyst

3.1.1 Effect of membrane type

As described in Chapter 2 and illustrated in Figure 3.1, the MPfRs had abiotic, H_2-based, and Pd-coated hollow fibers. Tests for composite and polypropylene were carried out separately after black Pd^0 was immobilized on the membrane. I set the H_2 pressure at 20 or 10 psig (2.36 or 1.68 atm) for the polypropylene or composite membranes, respectively; these correspond to maximum H_2-delivery capacities of 280 and 1600 meq/m^2/day, respectively (Tang et al., 2012).

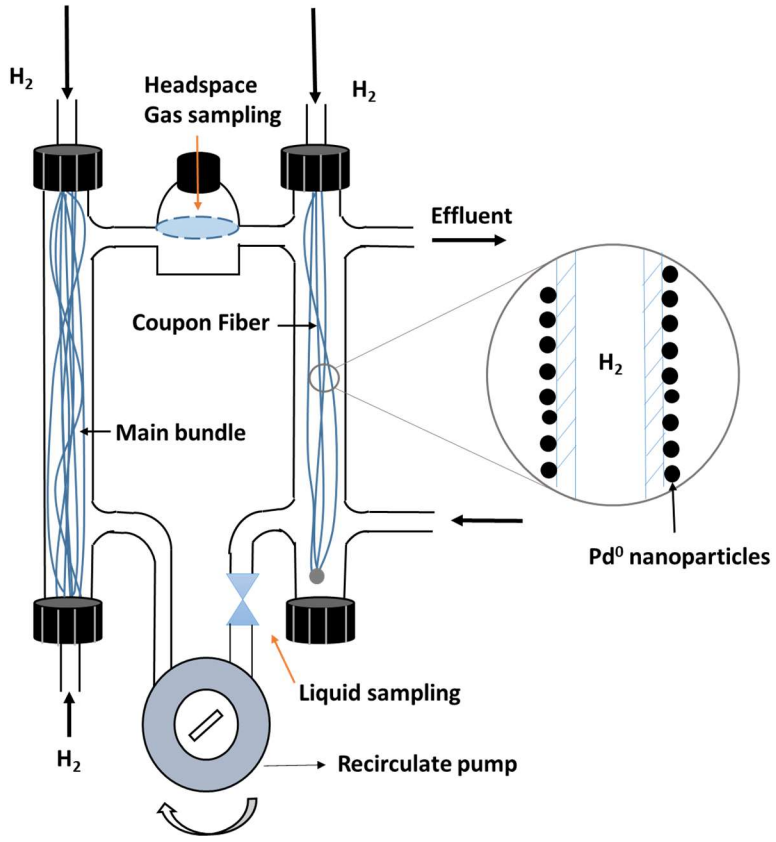

Figure 3.1. Schematic Diagram of the H2-based MPfR.

Figure 3.2 presents photographs of the Pd-coated membranes. The polypropylene and composite membranes showed very different coating patterns. The polypropylene membrane was entirely covered with small black Pd^0 particles, but the composite membrane was coated with bigger Pd^0 particles that only covered parts of the outer layer. Since the coating protocol was the same for both membrane types, the difference likely was caused by the difference in the H_2- delivery capacity: ~5-fold higher for the composite membrane than the polypropylene membrane. The higher H_2 flux led to a higher Pd^{2+} reduction rate and, perhaps, Pd autocatalysis (Zhou et al., 2016), resulting in agglomeration of larger Pd^0 particles. The small pores in the composite membrane's

outer layer also may have led to locally higher H_2 flux at the pores, resulting in high rate Pd autocatalysis and Pd agglomeration.

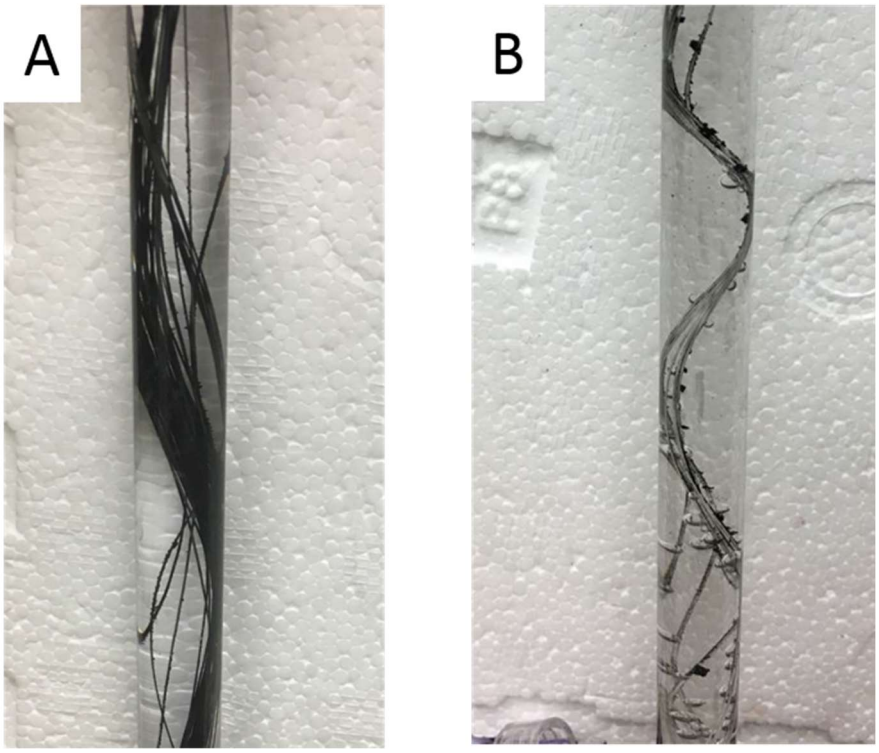

Figure 3.2. Photographs of Pd-coated (A) Polypropylene Membranes and (B) Composite Membranes.

The kinetics of NO_2^- reduction were used to evaluate the two hollow-fiber types since Pd is able to catalyze NO_2^- reduction (Zhou et al., 2017b). Compared to the single-wall polypropylene fiber, the composite fiber has higher H_2 permeability, which should have allowed higher contaminant surface loading, but it also resulted in more significant PdNP agglomeration, which may have lowered its effectiveness as a catalyst.

Two batch tests were performed in two MPfRs with different membranes at pH = 3. After the medium had been sparged with N_2 to eliminate O_2, 75-ml (the working volume of MPfR) was introduced to each MPfR. The starting concentrations of NO_2^- were about 1.3 mM. Batch experiments were carried out at room temperature (25°C), and 1.5-ml liquid samples were collected from the reactors every 10 minutes. NO_2^- concentrations were measured using anionic chromatography.

Figure 3.3 presents the results for NO_2^- reductions with the two membranes. NO_2^- removal was 99.9% for the composite membranes, but it was only 20% for the polypropylene membranes. The average removal rates were 1520 and 280 meq/ m^2-day, which correspond to the H_2 delivery capacities of 1600 and 300 meq/ m^2-day for the composite membranes and polypropylene membranes, respectively. Thus, Pd agglomeration did not slow NO_2^- reduction. The much slower removal rate for the polypropylene membranes apparently was due to their roughly 5-fold lower H_2-delivery capacity, and the difference in Pd^0 coating was not a major factor. Due to the superior performance, I used only the composite membranes in subsequent experiments.

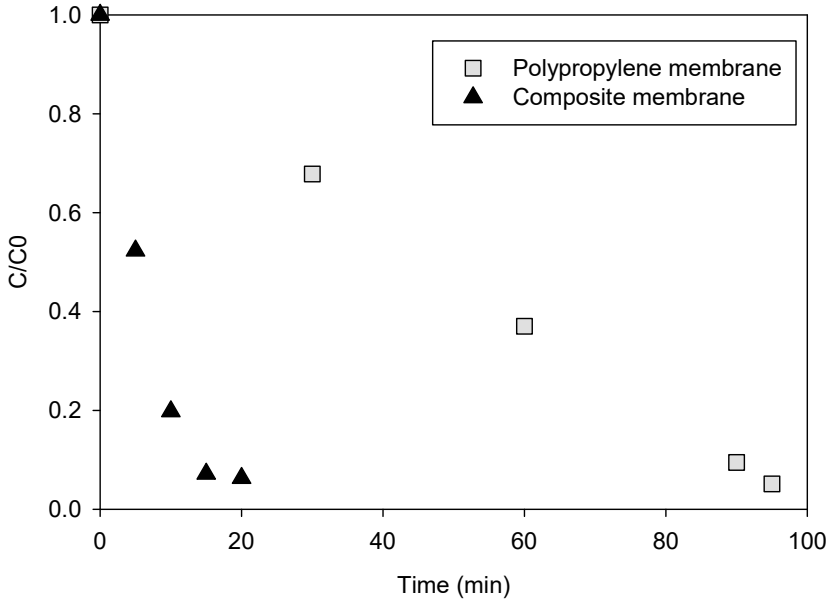

Figure 3.3. NO_2^- Reduction Catalyzed by Pd Coated on Polypropylene and Composite Membranes in Acidic Conditions.

3.1.2 Effect of H_2 pressure

To confirm the impact of H_2-delivery capacity, I conducted batch experiments with Pd-coated composite membranes using two H_2 pressure (4.5 and 10 psig, which equal 1.31 and 1.68 atm of absolute pressure) at neutral pH.

As shown in Figure 3.4, an initial concentration of 1.5 mmol/L NO_2^- was completely reduced in 60 minutes for both pressures. The NO_2^- concentration profiles were fit well by a pseudo-first-order kinetic model. The reduction rate constant $k_{(obs)}$ for 4.5 psig and 10 psig (1.31 atm and 1.68 atm) were the same, 0.08 min^{-1}. Thus, the H_2-delivery capacity was not an important factor for these experiments. Since H_2 delivery was not a

factor affecting the reaction rates, I set the H_2 pressure to 10 psig (1.68 atm) to ensure that H_2 would not be a limiting factor in the following tests.

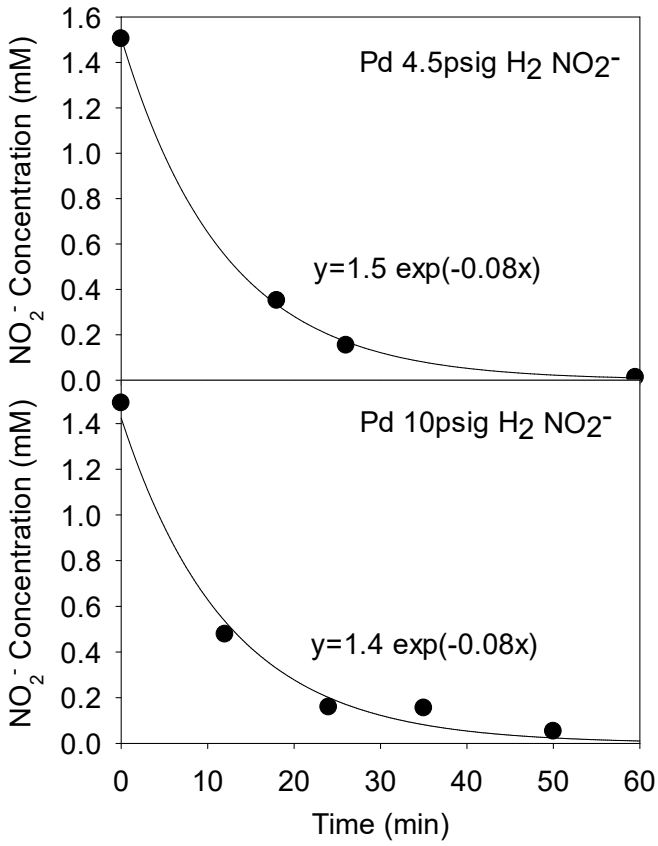

Figure 3.4. NO_2^- Reductions in Pd Composite Membranes at H_2 Pressure of 4.5 or 10 psig, which Correspond to 1.31 and 1.68 atm Absolute Pressure.

3.1.3 Effect of pH

I compared NO_2^- reductions in an acidic condition (pH = 3) and a neutral condition (pH = 7). 75 ml of 1.3-mM NO_2^- was added to the Pd-coated composite membrane reactor to begin a 60-minutes batch test. The H_2 pressure was 10 psig (1.68 atm), which corresponded to a H_2-delivery capacity of 1600 meq/m^2/day.

As shown in Figure 3.5, pH 3 gave much faster kinetics than pH 7: e.g., $k_{(obs)}$ of 0.16 min^{-1} versus 0.08 min^{-1}, or rate constant normalized by catalyst weight $k_{(cat.Pd)}$ 0.0007 $min^{-1}mgPd^{-1}$ versus 0.0004 $min^{-1}mgPd^{-1}$. NO_2^- reduction was faster at lower pH probably because (1) higher pH led to higher concentrations of OH^- and PO_4^{3-}, which compete with NO_2^- for the active adsorption sites at the catalyst surfaces (Prüsse & Vorlop, 2001), and (2) Pd-catalyzed NO_2^- reduction to N_2 needs to consume protons, which are at much higher concentration a lower pH:

$$NO_2^- + 1.5H_2 + H^+ = 0.5N_2 + 2H_2O$$

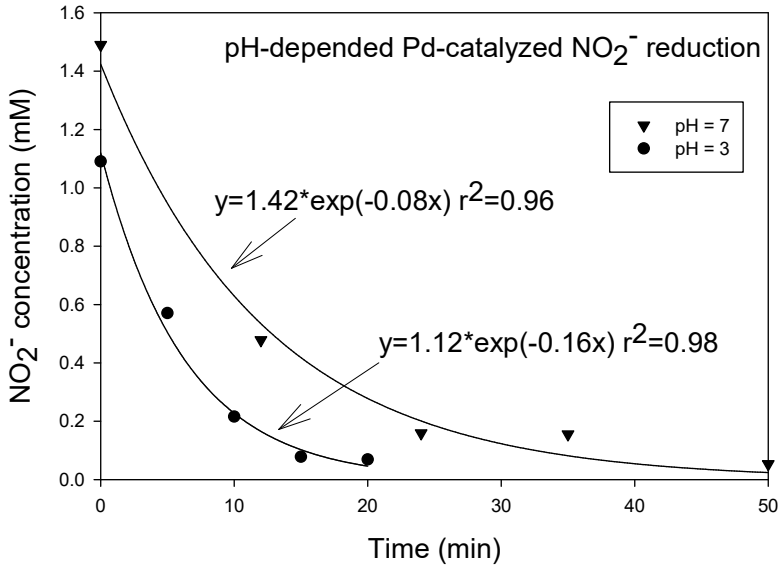

Figure 3.5. NO_2^- Reductions Catalyzed by Pd Coated on Composite Membranes at pH of 3 or 7 and H_2 Pressure of 10 psig (1.68 atm).

3.1.4 Insignificant reduction of ClO_4^-, ClO_3^-, or NO_3^- by Pd catalysis

I separately tested 0.1 mmol/L ClO_4^-, 0.1 mmol/L ClO_3^-, and 4 mmol/L NO_3^- in the MPfR. The reaction setups were the same as for NO_2^- reduction. The batches were conducted in anaerobic condition with 10 psig (1.68 atm) H_2 pressure and at neutral pH.

Reductions of ClO_4^-, ClO_3^-, and NO_3^- were negligible (<1% within 6 hours). This indicates that reductions of NO_3^- and ClO_4^- will require a secondary "promoter" metal, such as Cu (Sebastian Hörold, Tacke, & Vorlop, 1993; S Hörold, Vorlop, Tacke, & Sell, 1993), In (Prüsse et al., 2000), or Sn (B. P. Chaplin et al., 2012) with the Pd catalyst. One literature report showed ClO_3^- reduction catalyzed by monometallic Pd (X. Chen et al., 2017), and it may have been related to the form of Pd used or its having been coated on activated carbon.

3.2 Oxyanion Reduction Tests: Re-PdNPs as the Bimetallic Catalyst

3.2.1 pH-dependent NO_2^- reductions by Re-Pd catalysis

Since Pd on composite membranes did not catalyze ClO_3^-, ClO_4^-, or NO_3^- reduction, I turned to other synthesizing and coating catalysts on the composite membranes to test for ClO_4^- and NO_3^- reductions. Bimetallic Re-Pd was reported to catalyze ClO_4^- and ClO_3^- reductions efficiently (B. P. Chaplin et al., 2012; X. Chen et al., 2017; J. Liu et al., 2014). The reactor set up is explained in Chapter 2.

Reduction of 1.3-mM-NO_2^- in the Re-MPfR was studied for acidic (pH = 3) and neutral (pH = 7) conditions. As shown in Figure 3.6, >99.9% of the NO_2^- at the initial pH of 3 and <50% of NO_2^- at the initial pH of 7 was reduced within 20 minutes. The NO_2^--concentration profiles were fit well by pseudo-first-order kinetics. The reaction rate constants $k_{(obs)}$s were 0.16 min^{-1} and 0.04 min^{-1} at the pHs of 3 and 7, respectively. Normalized by catalyst weight, k(cat.Pd) were 0.0007 min^{-1} $mgPd^{-1}$ and 0.0002 $min^{-1}mgPd^{-1}$; k(cat.Re) were 0.0009 min^{-1} $mgRe^{-1}$ and 0.0002 min^{-1} $mgRe^{-1}$ at pHs of 3 and 7, respectively. That a solution pH of 7 slowed the reaction rate is consistent with the results of Pd catalysis.

Compared to NO_2^- reduction catalyzed by monometallic Pd (Fig. 3.5), NO_2^- reduction catalyzed by Re-Pd at pH = 7 was slower ($k_{(cat.Pd)}$ =0.0002 min^{-1} $mgPd^{-1}$) than by Pd ($k_{(cat.Pd)}$ = 0.0004 $min^{-1}mgPd^{-1}$). This difference probably occurred because Re had weak or no capability to catalyze the NO_2^- reductions. Thus, Re partially covered the Pd surfaces and resulted in fewer active sites for NO_2^- adsorption and subsequent reduction. When pH was 3, $k_{(cat.Pd)}$ for both catalysts was equal as 0.0007 $min^{-1}mgPd^{-1}$, which may have been due to the superior catalytic efficiency of Pd in acidic conditions overcame Re's effect.

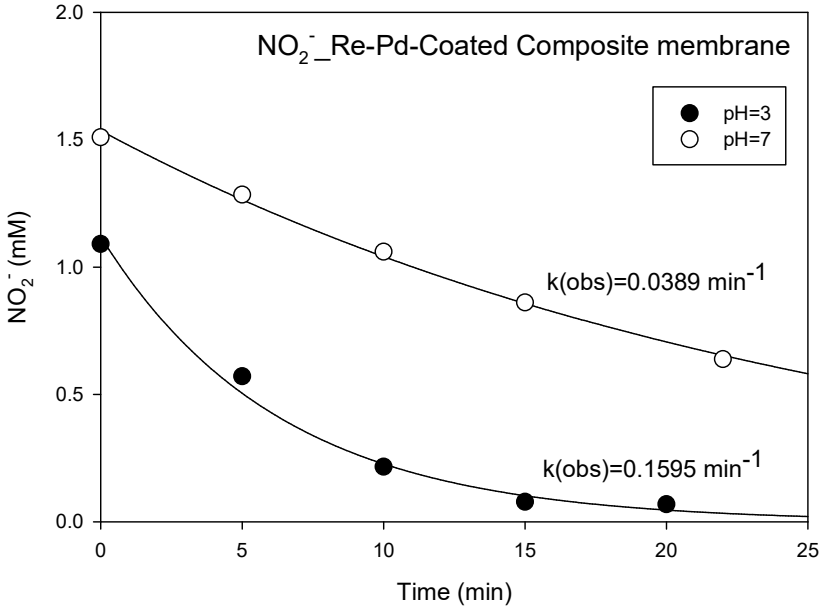

Figure 3.6. NO_2^- Reductions in the Re-MPfR at pH of 3 or 7 and H_2 Pressure of 10 psig (1.68 atm).

3.2.2 pH-dependent ClO_3^- reduction by Re-Pd catalysis

Three ClO_3^--reduction batch tests were performed in the Re-MPfR at pH of 4, 5.6, and 7. Figure 3.7 presents the ClO_3^--reduction results. In contrast to Pd, Re-Pd was able to catalyze ClO_3^- reduction: 99.9% of 1.1 mM ClO_3^- was reduced in 300 minutes when the pH was 4 or 5.6. The ClO_3^--concentration profiles were fit by pseudo-first-order kinetics. The reaction rate constants, $k_{(obs)}$, were 0.017 min^{-1} at pHs of 4 and 5.6 and 0.003 min^{-1} at pH of 7. This is consistent with the results of Pd catalysis for NO_2^- reductions, which indicates that the OH^- or PO_4^- might have competed with ClO_3^-. Shown in Figure 3.7, chloride ion (Cl^-) release gave a good mass balance with ClO_3^- loss.

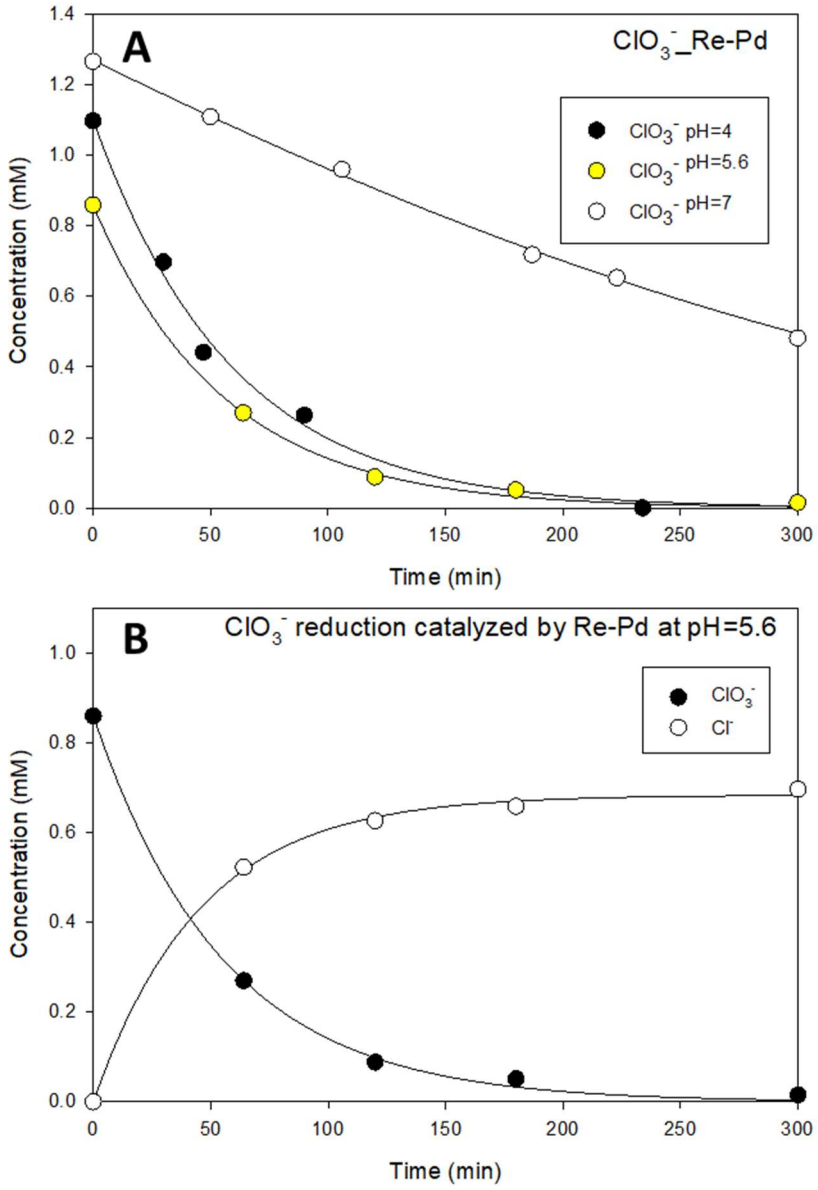

Figure 3.7. ClO_3^- Reductions in Re-MPfR. A: Reductions at pH of 4, 5.6, or 7 and H_2 pressure of 10 psig (1.68 atm). B: Mass balance of ClO_3^- reduction in Re-MPfR corresponding to A.

Comparing my results using Re-MPfR with other studies, the removal I observed in 30 minutes (<90% of 1 mM ClO_3^- at pH of 4) was much lower than Liu et al. (2014)

observed using $Re(hoz)_2$-Pd/C (99.9% of 1 mM ClO_3^- removed in 30 minutes at pH of 3). Normalized by Pd weight, $k_{(cat.Pd)}$ of $Re(hoz)_2$-Pd/C (0.03 $min^{-1}mgPd^{-1}$) was about 60-fold higher than that in my Re-MPfR (0.0005 $min^{-1}mgPd^{-1}$). Normalized by Re weight, reduction rate using $Re(hoz)_2$-Pd/C (0.03 $min^{-1}mgRe^{-1}$) was about 330-fold higher than that in my Re-MPfR (0.00009 $min^{-1}mgRe^{-1}$). The difference probably was due to using different forms of Re-Pd, as they may have different active sites.

3.2.3 Insignificant ClO_4^- or NO_3^- reduction by Re-Pd catalysis

In a batch experiment using ClO_4^- and NO_3^- in the Re-MPfR, no significant reductions of ClO_4^- or NO_3^- were catalyzed by Pd (<1% within 6 hours). This result does not correspond to the hypothetical reaction pathway (Fig. 3.8) reported in Hurley and Shapley (2007), in which ClO_4^- reduction was catalyzed. In the study of Hurley and Shapley (2007), Pd adsorbed H, while Re complexed perchlorate and released chloride through the transformation of four different Re complexes. Thus, a special form of catalysts is essential for the success of ClO_4^- reduction. My results suggest that Re-Pd formed on the membrane was not the same as in Hurley et al. (Hurley & Shapley, 2007).

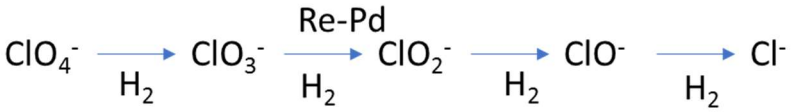

Figure 3.8. Hypothetical ClO_4^- Reduction Pathway (based on Hurley et al. (2007)).

3.3 Oxyanion Reduction Tests: Rh as the Monometallic Catalyst

3.3.1 NO_2^- reduction by Rh catalysis

NO_2^- reduction was evaluated in the Rh-reactor at neutral pH. As shown in Figure 3.9, NO_2^- reduction and removal was fit reasonably well by pseudo-first-order kinetics with a reaction constant normalized by catalyst weight of $k_{(cat.Rh)} = 0.0003\ min^{-1}mgRh^{-1}$, which is higher than Re-MPfR ($k_{(cat.Pd)} = 0.0002\ min^{-1}\ mgPd^{-1}$), but lower than MPfR ($k_{(cat.Pd)} = 0.0004\ min^{-1}mgPd^{-1}$). All three were capable of reducing NO_2^- at neutral pH and room temperature, while Pd showed higher activity than Rh (and Re-Pd) in the catalyzed reduction of NO_2^-. The catalysts' activity in my study does not correspond to the hydrogen chemisorption of each metal using the Sabatier principle (X. Chen et al., 2017; EPA, 1985; Restivo, Soares, Órfão, & Pereira, 2015), which considers Rh to be more active than Pd. I observed that Pd had higher reactivity for NO_2^- reduction, which reveals that hydrogen-chemisorption is not necessarily been the key controlling reactivity. The explanation for Pd's superior activity was that catalyst preparation was not optimized for individual metals (Rh or Re-Pd).

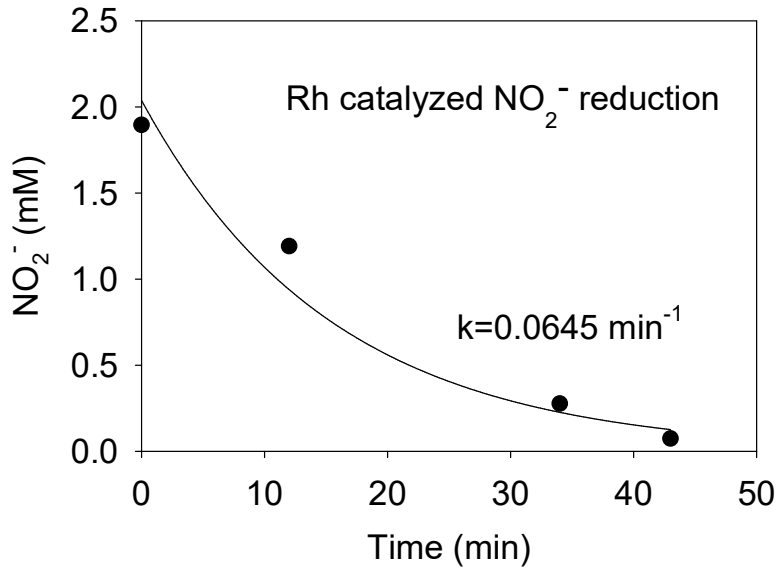

Figure 3.9. NO_2^- Reduction in Rh Reactor at Neutral pH and H_2 Pressure of 10 psig (1.68 atm).

3.3.2 ClO_3^- reduction by catalysis

I conducted three rounds of anaerobic batch tests of 0.1 mmol/L ClO_3^- in the Rh reactor at pH = 7 and 10 psig (1.68 atm) H_2 pressure. Figure 3.10 shows that the loss of ClO_3^- was fit well by pseudo-first-order kinetics. The first round batch showed 60% ClO_3^- reduction in 300 minutes and $k_{(obs)}$ was 0.0037 min^{-1}. Subsequent batches had slower kinetics, with $k_{(obs)}$ declining to 0.009 min^{-1} by batch 3. Brian P Chaplin, Roundy, Guy, Shapley, and Werth (2006) observed that a Cl^- concentration of 50 mg/L decreased the NO_3^- reduction by Pd-Cu; J. Liu et al. (2014) also observed a decrease of Re-Pd catalyzed ClO_4^- reduction rates, which they attributed to the gradual buildup of Cl^-. I hypothesize that Cl^- might have bonded to Pd sites by forming either (1) weak interactions with the catalyst metals, which was reversible upon rinsing catalysts with

deionized water, or (2) forming $RhCl_3$ and $RhCl_4^-$ species by stabilizing Pd^{2+} on the catalyst, which created irreversible deactivation.

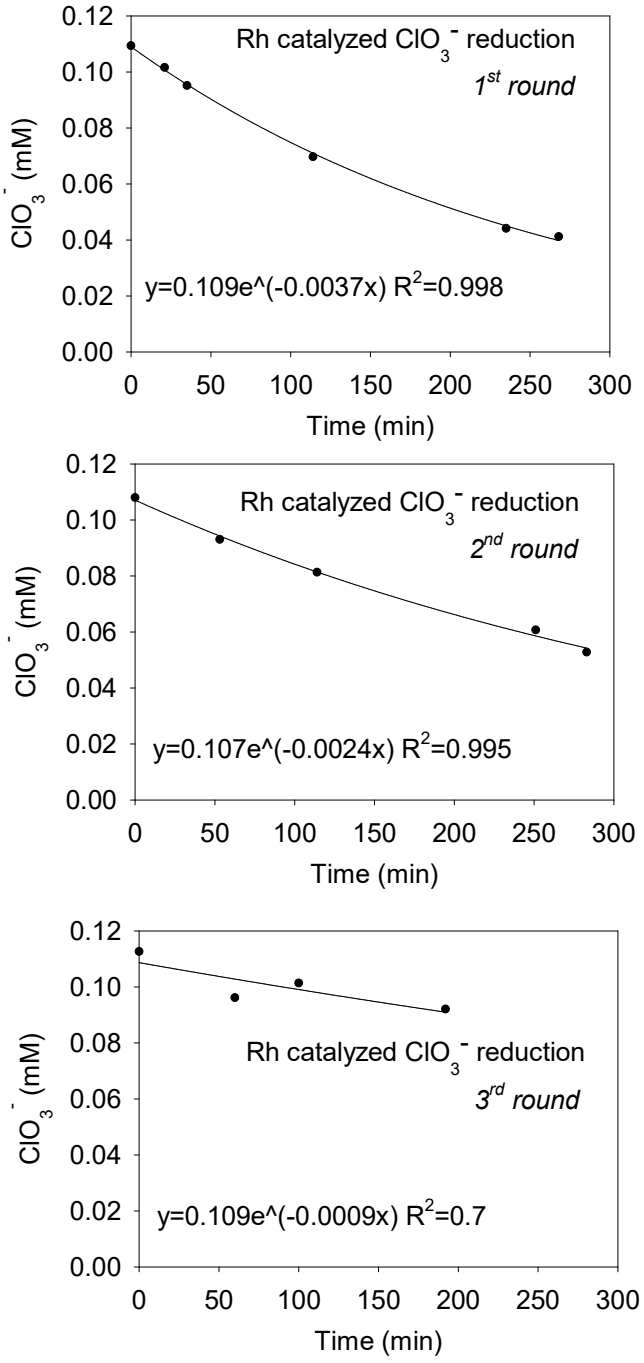

Figure 3.10. Sequential ClO_3^- Reductions in the Rh Reactor at Neutral pH and H_2 Pressure of 10 psig (1.68 atm).

3.4 Oxyanion Reduction Tests in Biotic Reactors

3.4.1 Continuous-flow mode oxyanions treatment in the MBfR and Pd-MBfR

As Pd proved to be the best choice, I used Pd in the biotic experiments described in Chapter 2. The MBfR and Pd-MBfR were operated in a continuous-flow mode at room temperature (~25°C) according to the series of conditions shown in Table 2-1. The goal was to find the operational conditions allowing good removal of oxyanions and energetics. A synthetic groundwater containing 4-mM NO_3^- and 0.1-mM ClO_4^- was supplied to both reactors during the first 5 stages, and a synthetic ammunition wastewater containing 4-mM NO_3^- and 2-mM ClO_4^- was supplied in the last stage. The final stage was designed to find operational conditions allowing the removal of oxyanions and energetics.

Low surface loading (SS1-SS5)

I set the influent rate at 0.04 ml/min and gradually increased it to 0.08 ml/min over the first 100 days. After the biofilms became mature, I introduced 2 mM of soluble Pd (as Na_2PdCl_4) into one of the reactors and allowed batch conditions to precipitate and immobilize black Pd^0 on the fiber bundles over one day; this created the Pd-MBfR. After five months, the reactors reached their first steady state (SS1). I then increased the flow rate to 0.17 ml/min, 0.211 ml/min, and finally to 0.3 ml/min, with corresponding increases of surface loading from 250 meq/m^2/day (SS1) to 600 meq/m^2/day (SS2), 800 meq/m^2/day (SS3), and then 900 meq/m^2/day (SS4 and SS5) after each previous steady

state. I coated Pd^0 again after SS4 to guarantee that Pd was covering the biofilm. After coating Pd^0 again, the MBfR and Pd-MBfR reached SS5.

Figures 3.11 and 3.12 show the NO_3^- and ClO_4^- concentrations for the first five stages in MBfR and Pd-MBfR, respectively. The NO_3^- and ClO_4^- fluxes for the steady states in both reactors are summarized in Table 3-1. All stages had higher-than-demand H_2 delivery so that H_2 availability was not a limiting factor and theoretically did not control the reaction rates.

As the flow rate and surface loading increased during SS1 to SS4, the removals of NO_3^- and ClO_4^- decreased in both reactors. The decrease of ClO_4^- removal was more significant than that of NO_3^-, which supports that NO_3^- reduction had priority over ClO_4^- reduction. NO_2^- was not detected in any reactors, and selectivity was at least 98% to N_2, as an insignificant amount (<0.5 mg/L) NH_4^+ was detected.

Differences between MBfR and Pd-MBfR were not obvious. Removals of NO_3^- and ClO_4^- exceeded 90% in both reactors.

To test if Pd had been flushed out of the Pd-MBfR during the first four steady states, I coated Pd again to Pd-MBfR (SS5). However, steady-state removals in Pd-MBfR remained similar to those of the MBfR. (Both reactors showed higher percentage removals, which were caused by a pH adjustment from 7.8 to 7.2).

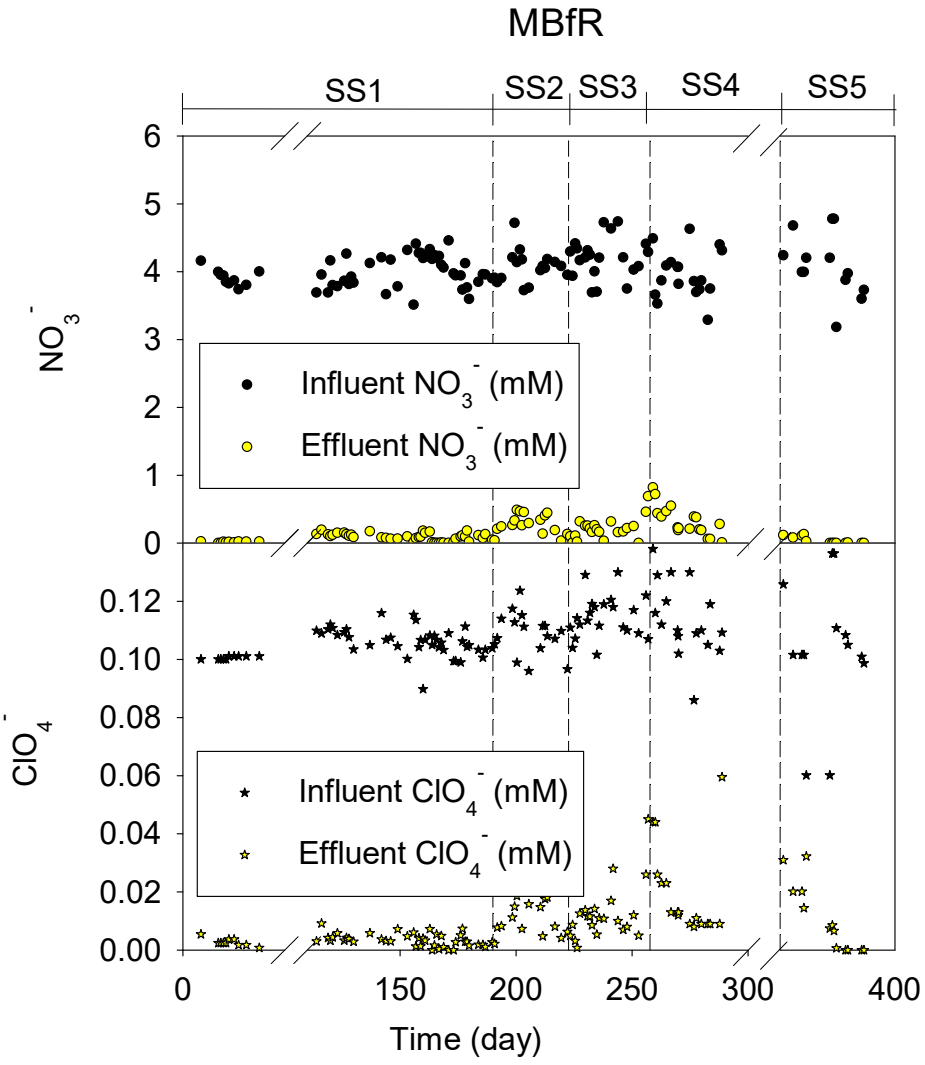

Figure 3.11. Performance Profiles for Five Conditions of the MBfR Fed NO_3^- and ClO_4^-. Top: Measured NO_3^- influent and effluent concentration in MBfR. Bottom: Measured ClO_4^- influent and effluent concentration in MBfR.

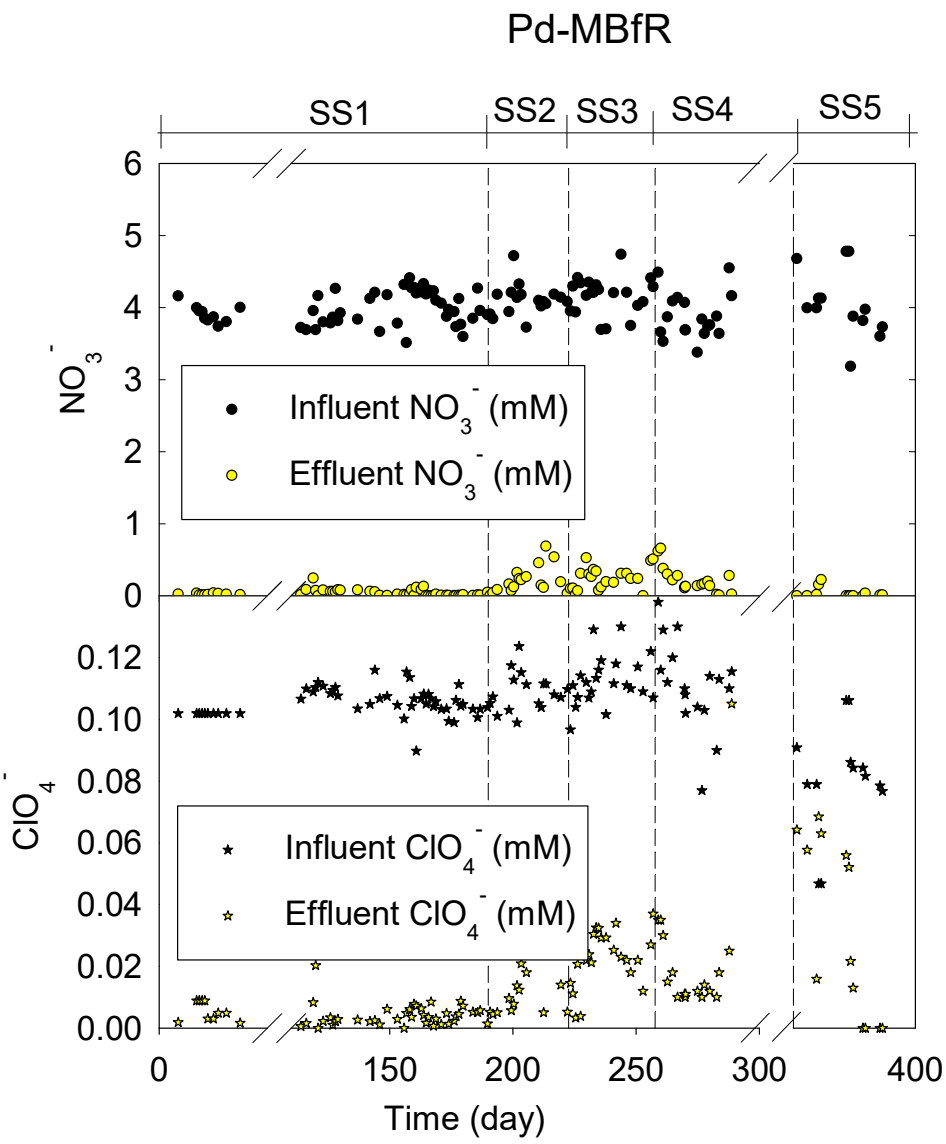

Figure 3.12. Performance Profiles for Five Conditions of the Pd-MBfR Fed NO_3^- and ClO_4^-. Top: Measured NO_3^- influent and effluent concentrations in Pd-MBfR. Bottom: Measured ClO_4^- influent and effluent concentrations in Pd-MBfR.

High surface loading (SS6)

In stage 6, when I fed the reactor continuously with a higher ClO_4^- concentration (2 mM ClO_4^-), the reactors experienced sharp increases of surface loading to 1700

meq/m^2/day. I increased the H_2-delivery capacity from 1250 meq/m^2/day to 2500 meq/m^2/day by increasing the H_2 pressure from 10 psig (1.68 atm) to 20 psig (2.36 atm). Thus, the H_2 supply still was sufficient for full reductions of NO_3^- and ClO_4^-.

Figures 3.13 and 3.14 show the performance during the first 60 days of stage 6 for the MBfR and Pd-MBfR. NO_3^- was completely removed in the MBfR and the Pd-MBfR. Negligible NH_4^+ (< 0.5 mg/L) was detected during the experiments. Unlike the low-surface-loading stages, the MBfR and Pd-MBfR could only remove about one-half of the 2-mM ClO_4^- in the presence of NO_3^-. During SS6, ClO_4^- removal decreased significantly, to 63% in MBfR and 60% in Pd-MBfR; this was coincident with an increase of the influent ClO_4^- concentration from 0.1 mmol/L to 2 mmol/L. The similar ClO_4^- removal in the MBfR and Pd-MBfR confirmed the results in the MPfR that Pd did not catalyze ClO_4^- reduction. What's more, Pd coated in the biofilm hindered ClO_4^- reduction, perhaps because of its toxicity to the biofilm (Wataha & Hanks, 1996).

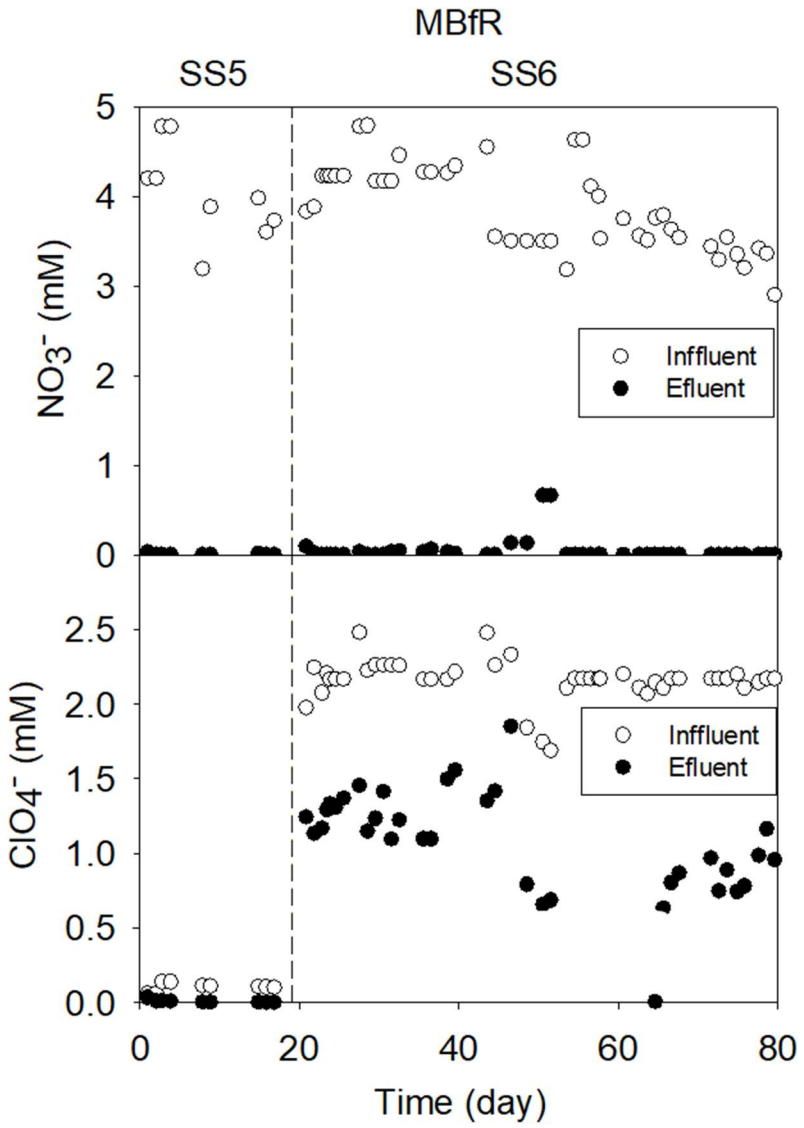

Figure 3.13. Performance Profiles in the MBfR in Steady States 5 and 6. The ClO_4^- loading was increased 20-fold for SS6. Top: Measured NO_3^- influent and effluent concentrations in MBfR. Bottom: Measured ClO_4^- influent and effluent concentrations in MBfR.

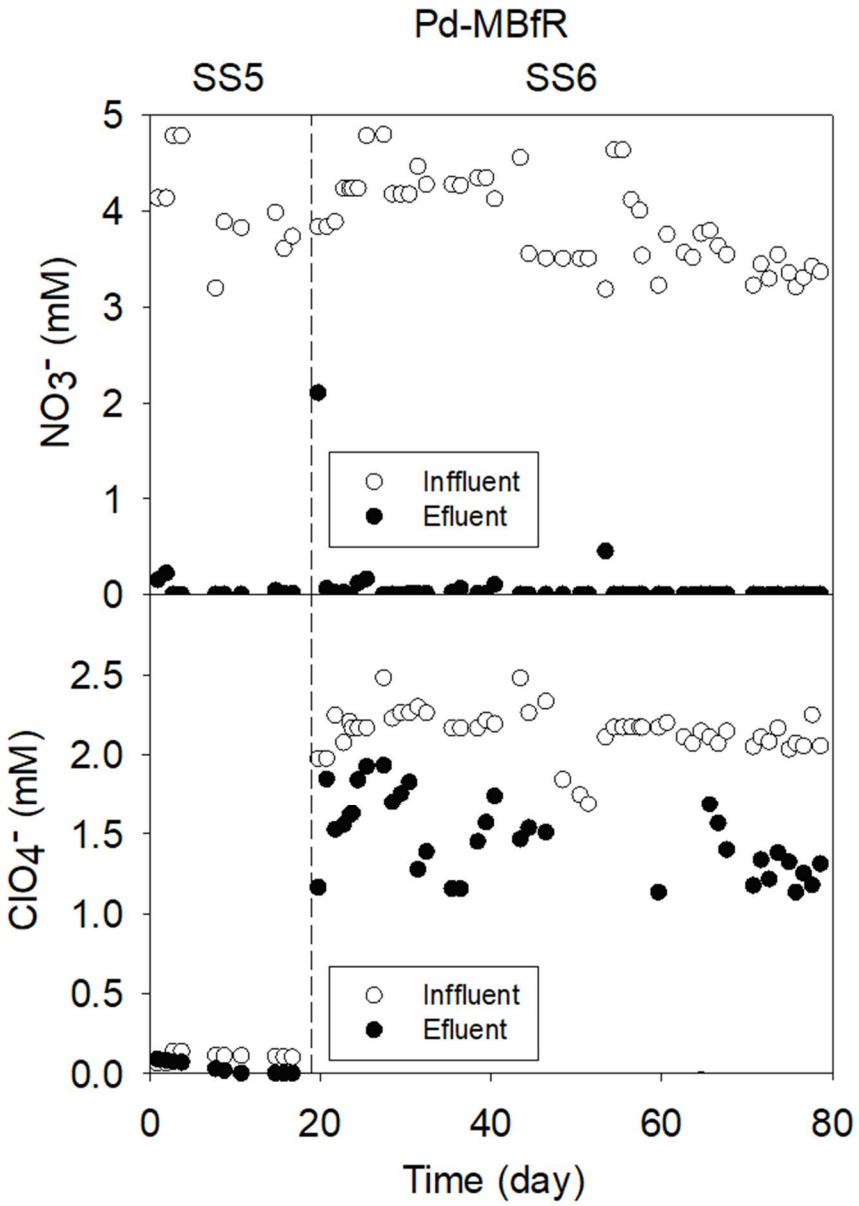

Figure 3.14. Performance Profiles in the Pd-MBfR in Steady States 5 and 6. The ClO_4^- loading was increased 20-fold for SS6. Top: Measured NO_3^- influent and effluent concentrations in Pd-MBfR. Bottom: Measured ClO_4^- influent and effluent concentrations in Pd-MBfR.

3.4.2 Summary of stages

Table 3-1 summarizes the results for the steady states of stages 1 – 6. As the flow rate and acceptor surface loading increased, the removal of NO_3^- decreased in both reactors during SS1 to SS3. The decrease of ClO_4^- removal was more significant than that of NO_3^-, which supports that NO_3^- reduction had higher priority over ClO_4^- reduction in this system. NO_2^- was not detected in any reactors. NO_3^- in the Pd-MBfR had greater than 98% selectivity to N_2, as an insignificant amount (<0.5 mg/L) NH_4^+ was detected.

Differences between MBfR and Pd-MBfR were not large. Removals of NO_3^- and ClO_4^- in both reactors were as high as about 90% and sometimes more. To test if Pd had been flushed out of the Pd-MBfR, I coated Pd again to the Pd-MBfR for SS5. However, removal at steady state for the Pd-MBfR remained similar to that of the MBfR. Both had increased removals due to a pH adjustment from 7.8 to 7.2.

The ClO_4^- percentage removal decreased significantly, from more than 90% to 63% in the MBfR and to 60% in the Pd-MBfR after raising ClO_4^- concentration from 0.1 mmol/L to 2 mmol/L (SS6). This suggests that Pd was not playing a significant role in ClO_4^- reduction in the presence of NO_3^-, which is consistent with what I observed in the abiotic reactors. If fact, the slightly smaller ClO_4^- remove in Pd-MBfR suggests that the Pd^0 may have covered the biomass, resulting in less biofilm.

Table 3-1. Fluxes of H_2, NO_3^-, and ClO_4- for the Six Steady States

Steady state	NO_3^- surface loading mEq/m^2-day		NO_3^- Flux mEq/m^2-day		ClO_4^- surface loading mEq/m^2-day		ClO_4^- Flux mEq/m^2-day	
(SS)	MBfR	Pd-MBfR	MBfR	Pd-MBfR	MBfR	Pd-MBfR	MBfR	Pd-MBfR
SS1	240	240	240	240	10	7	10	7
SS2	550	550	520	540	24	24	22	20
SS3	740	740	710	710	31	42	27	34
SS4	950	950	870	860	43	37	38	33
SS5	906	906	910	855	39	39	39	37
SS6	910	910	910	910	810	830	520	490

3.4.2 Batch mode oxyanions treatment in MBfR and Pd-MBfR

I tested ClO_4^-, ClO_3^-, NO_3^-, and NO_2^- reduction kinetics in the MBfR and Pd-MBfR using batch tests at the end of steady state 1, 5, and 6. The batch tests were conducted at pH 7 and room temperature (25°C) in anaerobic conditions. H_2 pressures were 5 psig (1.34 atm) for SS1, 10 psig (1.68 atm) for SS5, and 20 psig (2.36 atm) for SS6. Contaminant concentrations depended on the medium used in the corresponding stages.

Figure 3.15 presents ClO_4^- reductions in the MBfR and Pd-MBfR after SS1. For both reactors, reaction rates were slow in the first 20 minutes, increased from 20 to 60 minutes and slowed during the last 40 minutes. The retarded ClO_4^- reduction at first 20 minutes may have been because of the presence of O_2 remaining in the reactor or introduced with the influent, which has priority over ClO_4^- as an e^- acceptor. Transient accumulation ClO_3^- (up to 20% of the initial ClO_4^-) was detected during the batch. Chloride ion (Cl^-) release had a good mass balance with ClO_4^- and ClO_3^- loss. The ClO_4^- reduction from the 20th minute was fit well by pseudo-first-order kinetics. The reaction

constants for the MBfR and the Pd-MBfR were equal as 0.024 min^{-1}, which indicates that Pd did not catalyze the ClO_4^- reductions.

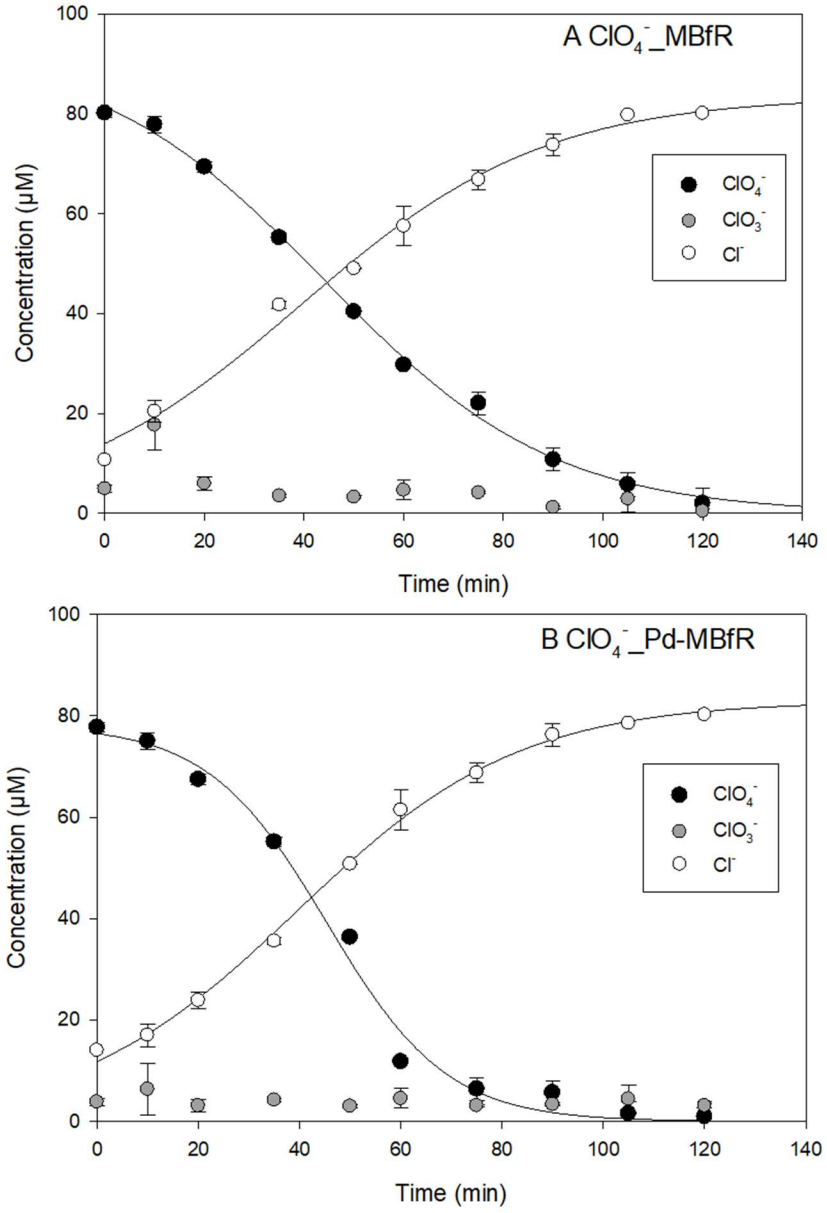

Figure 3.15. Profiles of ClO_4^- Reduction in Batch Mode (SS1) (A): MBfR, (B): Pd-MBfR.

Figure 3.16 presents ClO_3^- reductions in the MBfR and Pd-MBfR. ClO_3^- reductions in MBfR and Pd-MBfR had similar trends with ClO_4^- reductions. Except for hindered ClO_3^- reduction (by O_2) in the first 20 minutes, the reductions were fit well by pseudo-first-order kinetics: $k_{(obs)}$ values for the MBfR and Pd-MBfR were 0.022 min^{-1} and 0.026 min^{-1}, respectively. Chloride ion release matched with ClO_3^- ion loss with a good mass balance.

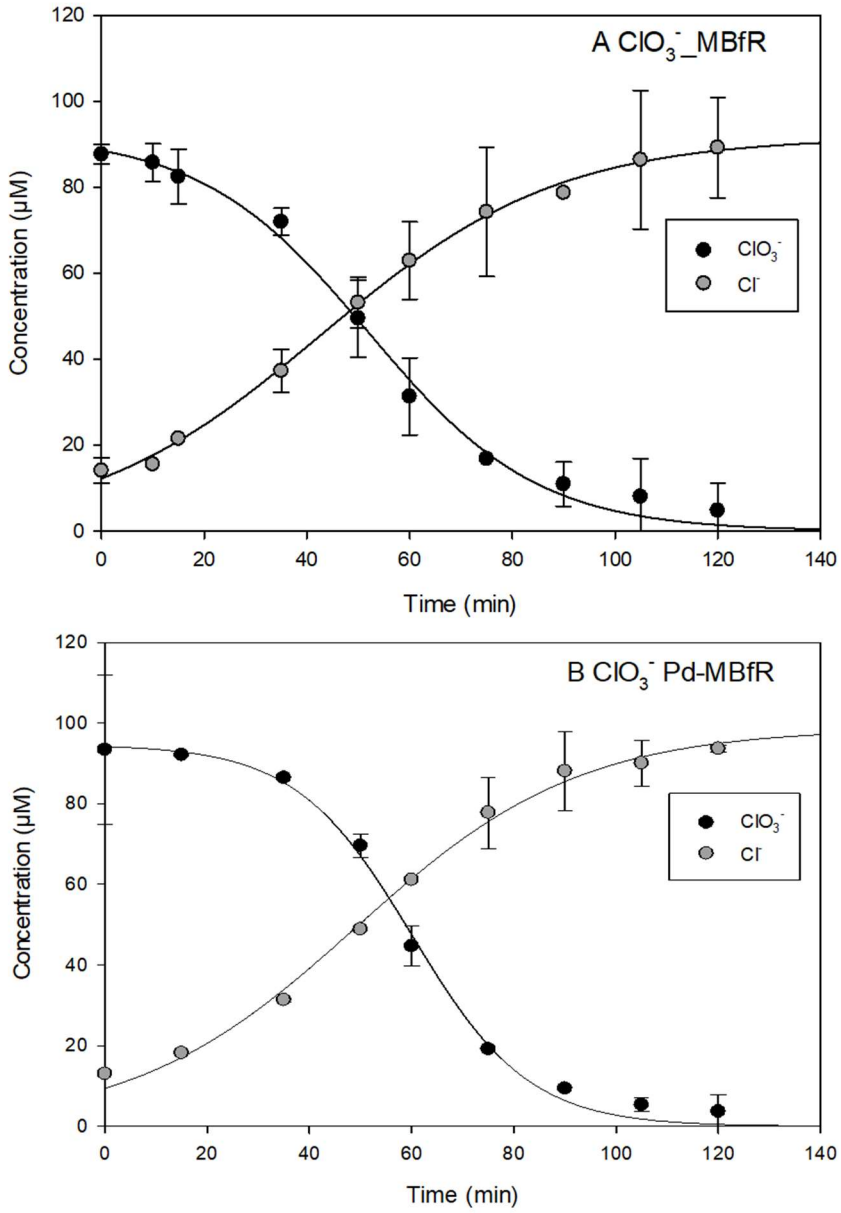

Figure 3.16. Profiles of ClO_3^- Reduction in Batch Mode (SS1) (A): MBfR, (B): Pd-MBfR.

4 mM NO_3^- was introduced to the reactors for the batch test. <50% of the NO_3^- was reduced in 80 minutes (Fig. 3.17) in both reactors. The reductions could be fit by pseudo-first-order kinetics: $k_{(obs)}$ value for the Pd-MBfR and the MBfR were the same

($k_{(obs)}$ = 0.011 min^{-1}). Since Pd did not catalyze the NO_3^- reduction, the higher reduction rates in Pd-MBfR might have been because Pd catalyzed NO_2^- reduction, which accelerated the overall reaction. I conducted NO_2^--reduction tests were to verify the hypothesis.

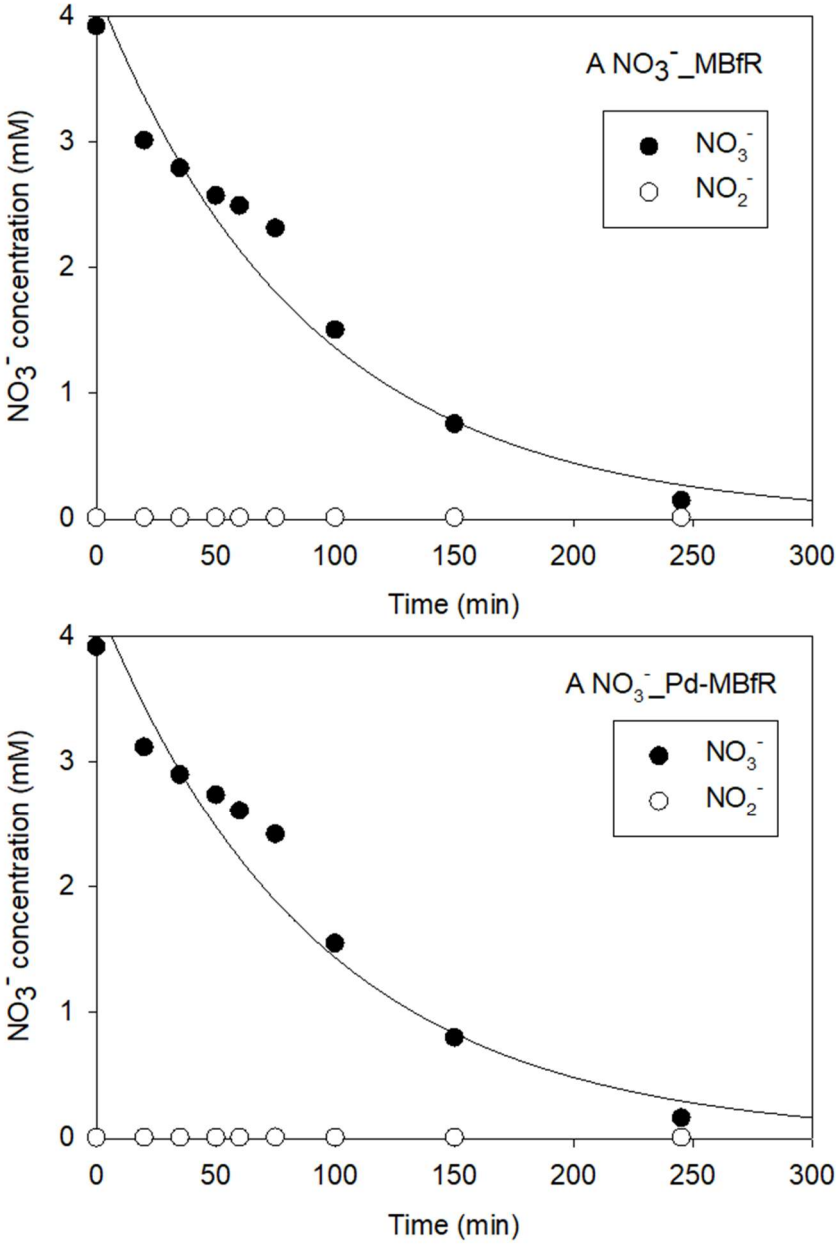

Figure 3.17. Profiles of NO_3^- Reduction in Batch Mode (SS1) (A): MBfR, (B): Pd-MBfR.

When 4 mM NO_2^- was introduced to the reactors, about 70% of the NO_2^- was reduced in 160 minutes in each reactor (Fig. 3.18). The pseudo-first-order rate constant

for the MBfR was 0.006 min^{-1}, but it was higher than for the Pd-MBfR (0.004 min^{-1}). Although the NO_2^- results do not explain the results for NO_3^- reductions, it is consistent with the results shown in continuous tests. This suggests that NO_2^- reduction may not have been catalyzed by Pd in the MBfR in this test. However, it contrasts with the results shown in NO_2^- reduction conducted in Pd-coated composite membranes reactor that NO_2^- reduction may be catalyzed by Pd coated on composite membranes. Two explanation are possible for the differences: 1) Pd was partially flushed out of the MBfR, and the remaining Pd was not enough to significantly catalyze NO_2^- reduction; or 2) Pd was covered by grown biofilms such that NO_2^- was blocked from adsorption sites on the Pd surfaces.

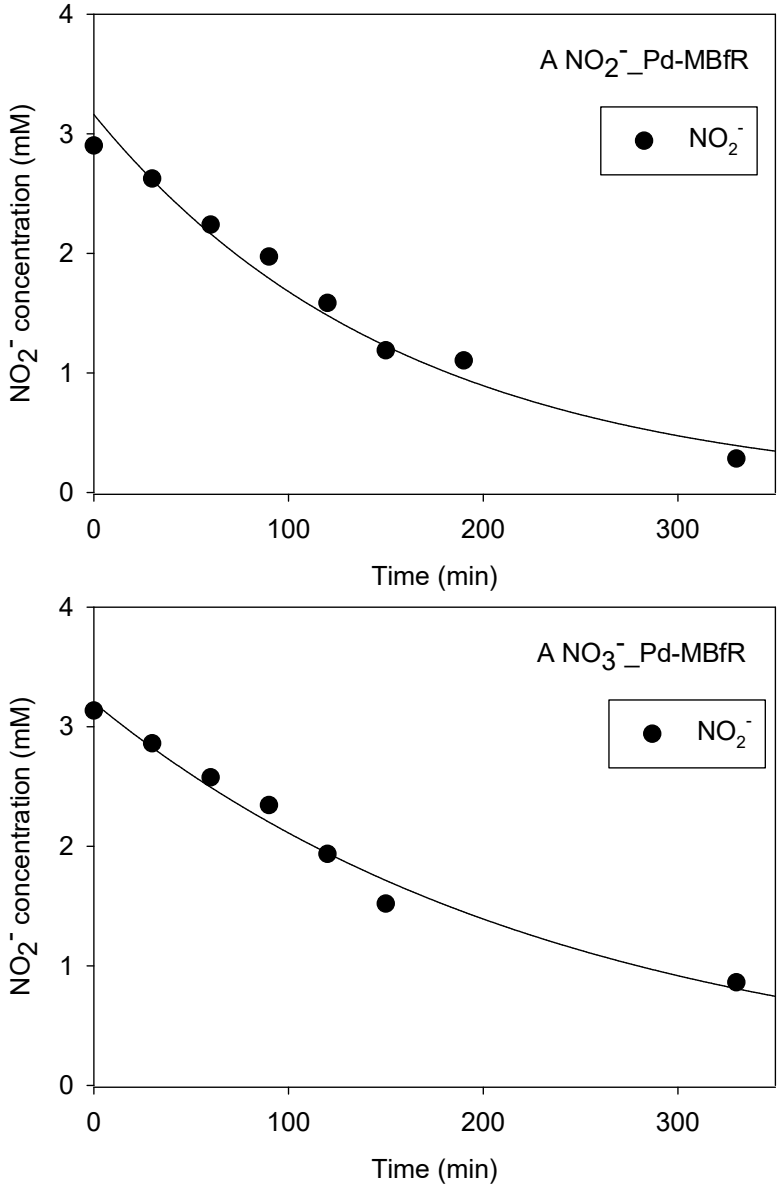

Figure 3.18. Profiles of NO_3^- Reduction in Batch Mode (SS1) (A): MBfR, (B): Pd-MBfR.

$k_{(obs)}$ values for steady states 1, 5, and 6 are summarized in Table 3-2. In most cases, Pd-MBfR did not improve the removal rates of the four contaminants over the MBfR,

probably because the biofilm out-competed Pd for these four e^- acceptors. Reduction rates of NO_3^- and NO_2^- significantly increased with the surface loading increased from stage-1 (250 meq/m^2/day), to stage-5 (900 meq/m^2/day), and then to stage-6 (1700 meq/m^2/day). In contrast, ClO_4^- reduction rates decreased from 0.024 min^{-1} to 0.002-0.003 min^{-1} after the ClO_4^- surface loading was increased. This might have been because the high ClO_4^- concentration (2 mM) hindered biofilm function, resulting in slower reduction rates. The ClO_3^- reduction rates did not decrease until I fed 2 mM ClO_4^-, which indicates that 2-mM ClO_4^- had adverse effects on biofilm. In contrast, 3-fold higher ClO_4^- (0.3-mM) was removed in 120 minutes in stage-6 compared with stage-1 (0.1-mM), which corresponded to the ClO_4^- flux increase from 40 meq/m^2/day to 500 meq/m^2/day in continuous-flow mode.

Table 3-2. $k_{(obs)}$ Values for NO_3^-, ClO_4^-, NO_2^-, and ClO_3^- Reductions in the MBfR and the Pd-MBfR

Steady State	MBfR				Pd-MBfR			
(min^{-1})	NO_3^-	ClO_4^-	NO_2^-	ClO_3^-	NO_3^-	ClO_4^-	NO_2^-	ClO_3^-
SS2	0.011	0.024	0.006	0.022	0.010	0.024	0.004	0.026
SS5	0.017	0.027	0.023	0.085	0.017	0.020	0.028	0.082
SS6	0.038	0.003	0.040	0.020	0.027	0.002	0.016	0.008

3.5 Conclusion

Pd was the best choice among the three metal catalysts – Pd, Pd-Re, and Rh -- in three ways: (1) Pd-Re had a low catalysts efficiency for ClO_3^- reductions compared with

other studies; (2) Since the released Cl^- ions blocked active sites, Pd-Re or Rh was deactivated with repeated tests; and (3) Pd had the highest reactivity for NO_2^- reductions.

The metal-catalyzed reductions of the oxyanions were affected by the H_2-delivery capacity and pH. H_2 supplied through the composite membrane improved reduction rates significantly, since the composite membrane has a 10-fold higher maximum flux than the polypropylene membrane at the same H_2 pressure. For pH-dependent oxyanion reductions by metal catalysts, lower pHs gave higher reduction rates, probably because OH^- compete with the oxyanions for the active sites on the catalysts surface at higher pH.

Biotic reactors showed stable capacity to removal oxyanions. The MBfR and the Pd-MBfR had greater than 90% removal for 4 mM NO_3^- and 60% removal for 2 mM ClO_4^-. However, Pd catalysts coupled with biofilm did not catalyze the oxyanions reductions, probably because the biofilms covered the Pd's adsorption sites.

ENERGETICS TREATMENT IN THREE REACTORS

4.1 Degradability of RDX/HMX in Three Reactors

I conducted tests for two energetics, RDX and HMX, in the Pd-film reactor, MBfR, and Pd-MBfR at the end of steady state 6 (SS6). The batch tests were conducted at pH = 7 and 25℃ in anaerobic conditions. The H_2 pressure was 20 psig (2.36 atm).

Figure 4.1 presents the reduction profiles for RDX (top) and HMX (bottom) in the MBfR. RDX or HMX concentrations are plotted as closed black circles, while open circles are for NO_2^-. The initial concentrations (C_0) for RDX and HMX were 20 mg/L.

I fit the decreasing concentration of RDX and HMX with pseudo-first-order kinetics:

$$C_t/C_0 = e^{-k(obs)t}$$

C_t is the concentration in μmol/L at t-minute, C_0 is the initial concentration (90 μmol/L for RDX or 70 μmol/L HMX), C_0 for N is determined by the total nitroamine groups (270 μmol/L N for RDX or 280 μmol/L N for HMX), and $k_{(obs)}$ is the first-order loss coefficient (min^{-1}).

Biodegradations of RDX and HMX were slow: in 60 minutes, less than 20% removal of 90 μmol/L (20 mg/L) RDX (k(obs) = 0.0025 min^{-1}) and less than 15% or 70 μmol/L (20 mg/L) HMX (k(obs) = 0.0017 min^{-1}). Since I detected up to 10 μmol/L NO_2^- (about 1/5 of the maximum NO_2^- that could have been denitrated from 20% of the initial 90 μmol/L RDX) during the process, I presume that the nitramine group was broken at its N-N bond:

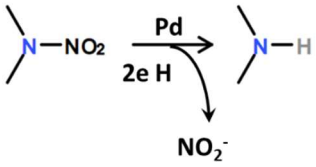

The results in Figure 4.1 suggest that direct biodegradation of RDX and HMX is not promising.

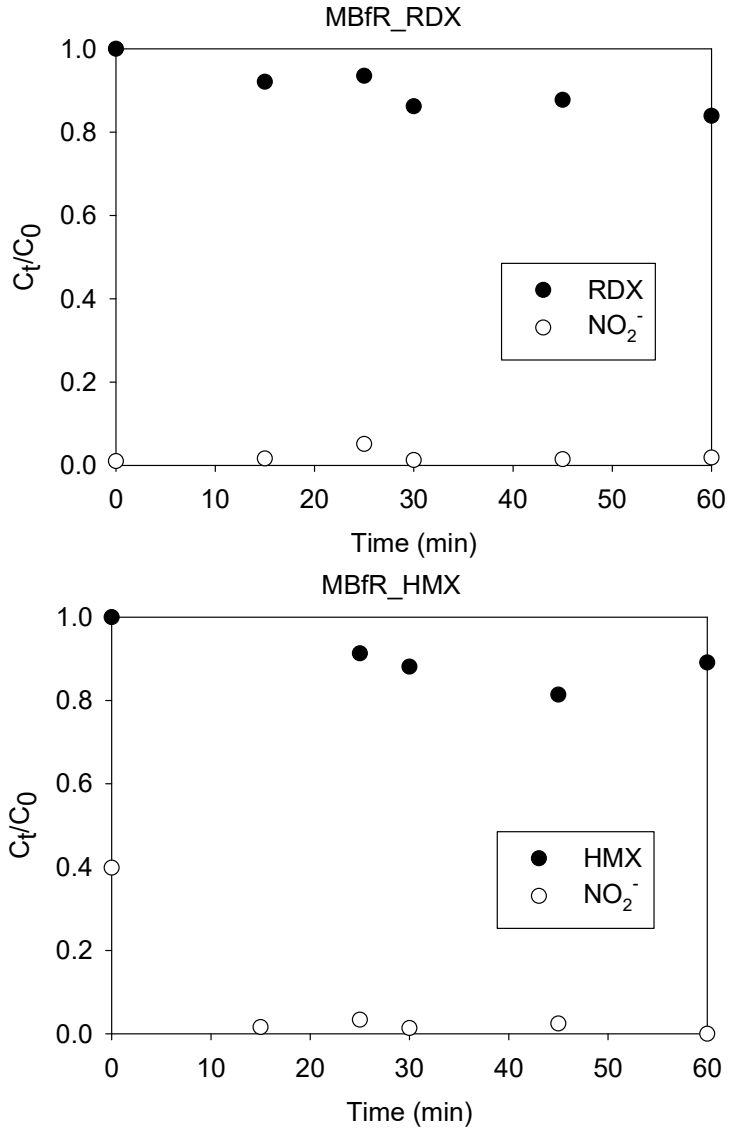

Figure 4.1. Biodegradation of RDX (Top) and HMX (bottom) in the MBfR with the Formation of NO_2^-.

Figure 4.2 shows that RDX and HMX were degraded much better in the MPfR: Both were completely removed in 60 minutes. RDX and HMX decompositions were accompanied with the accumulation of NO_2^-, which was reduced gradually. The b values were 0.136 min^{-1} and 0.079 min^{-1} for RDX and HMX, respectively. The slower reduction rate for HMX may have occurred because HMX has one more nitroamine group, which requires more electron equivalents to reduce. Compared with MBfR, the MPfR had a much higher rate in energetics denitration and NO_2^- accumulation.

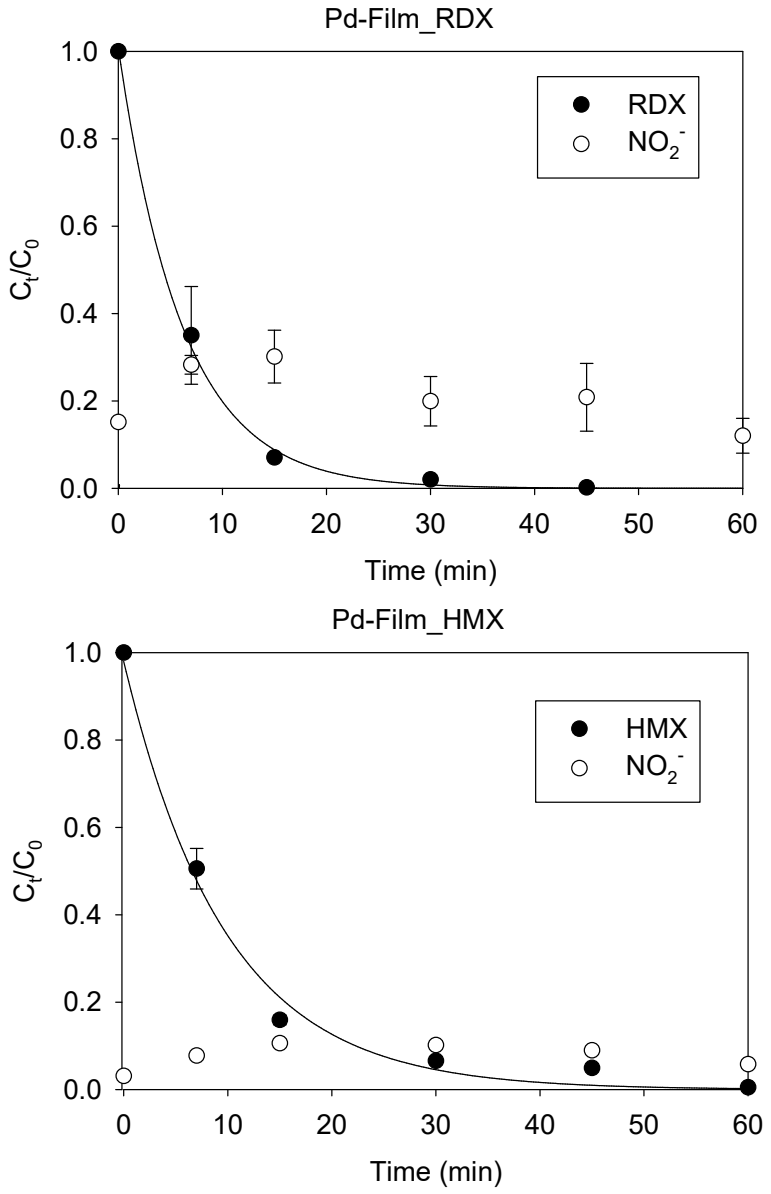

Figure 4.2. Degradation of RDX (top) and HMX (bottom) in the Pd-Film Reactor with Formation and Loss of Nitrite.

Figure 4.3 shows the losses of RDX and HMX in the Pd-MBfR. RDX was removed rapidly in 60 minutes and with almost no NO_2^- accumulation. The $k_{(obs)}$ values were 0.114 min^{-1} and 0.073 min^{-1} for RDX and HMX, respectively. Similar to the MPfR, the

decomposition rate of HMX was slower than for RDX. One difference is that NO_2^- did not accumulate in the Pd-MBfR.

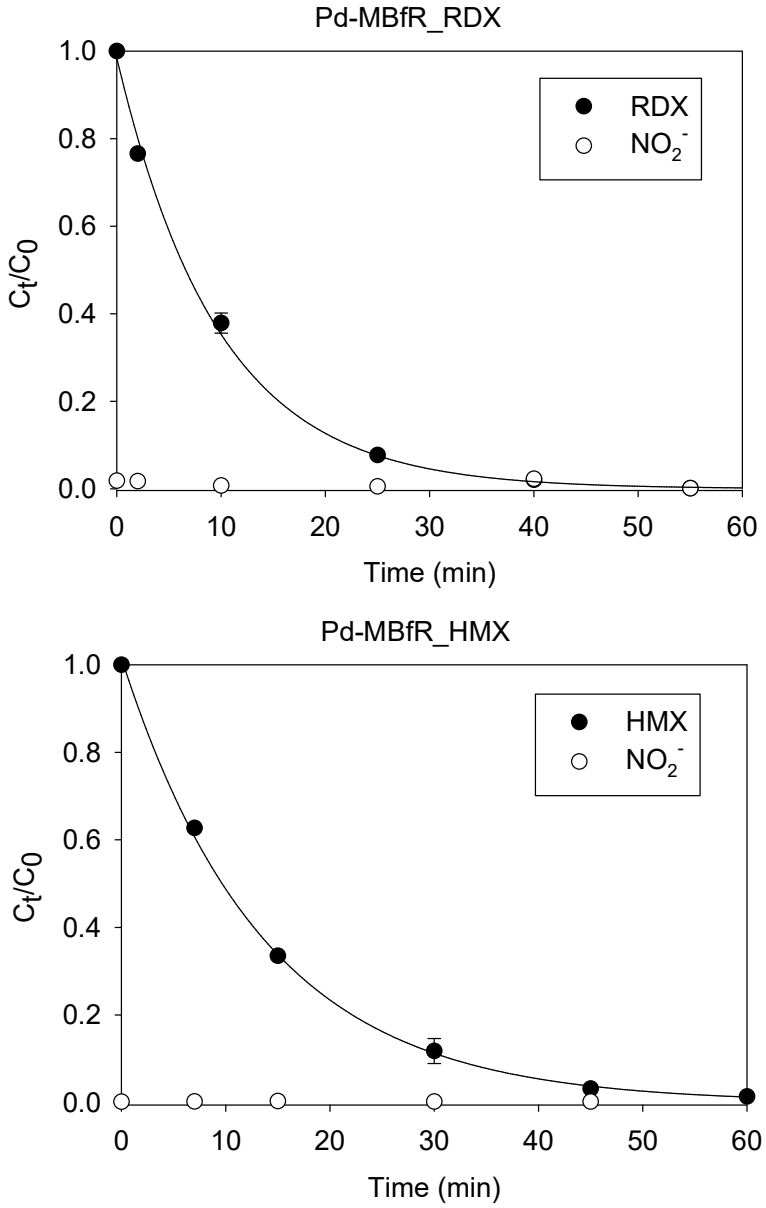

Figure 4.3. Biodegradation of RDX (top) and HMX (bottom) in Pd-MBfR.

Table 4.1 compares the kinetics for the MBfR, MPfR, and Pd-MBfR. The reaction rates were higher in the MPfR than in the Pd-MBfR and much higher than in the MBfR. Thus, Pd played the most significant role is the reduction of RDX and HMX, but the presence of biofilm slowed the rate to a modest degree. This may have been caused by biofilm accumulation blocking some active sited on the Pd catalyst.

Compared with the MPfR, much less NO_2^- accumulated in the Pd-MBfR, because the biofilm quickly reduced the NO_2^- released by denitration of RDX and HMX. Thus, the cooperation of Pd and biofilm guaranteed high removal rates and no accumulation of this undesired intermediate.

Table 4-1. $k_{(obs)}$ Values for RDX and HMX Reductions in the MPfR, MBfR and the Pd-MBfR

Energetics	MBfR	MPfR	Pd-MBfR
RDX	0.0025	0.136	0.115
HMX	0.0017	0.079	0.073

4.2 Degradability of RDX by Other Bimetal Catalysts

Research has been conducted on bimetallic formulations for catalyzing the reduction of energetics: e.g., Pt, Ru, Rh, and Au with Pd (X. Chen et al., 2017). I used an MPfR control (47 mg Pd) to evaluate the bimetallic catalysts (40 mg Pd with other catalysts) in comparison with the MPfR. The formation of bimetallic MPfRs is described in section 2.1.

Figure 4.4 presents the results of RDX degradation with the four bimetallic catalysts -- Pt-MPfR, Ru-MPfR, Rh-MPfR, and Au-MPfR -- and one Pd-film reactor as control. RDX was removed rapidly in 30 minutes in all five reactors. $k_{(obs)}$ values were 0.181 min^{-1}, 0.185 min^{-1}, 0.106 min^{-1}, 0.153 min^{-1}, and 0.194 min^{-1} for Pt-MPfR, Ru-MPfR, Rh-MPfR, Au-MPfR, and Pd-film reactor, respectively. Among the bimetallic catalysts, Pd/Ru had the lowest reactivity, while Pd/Rh had the highest reactivity. Pd alone was the fastest.

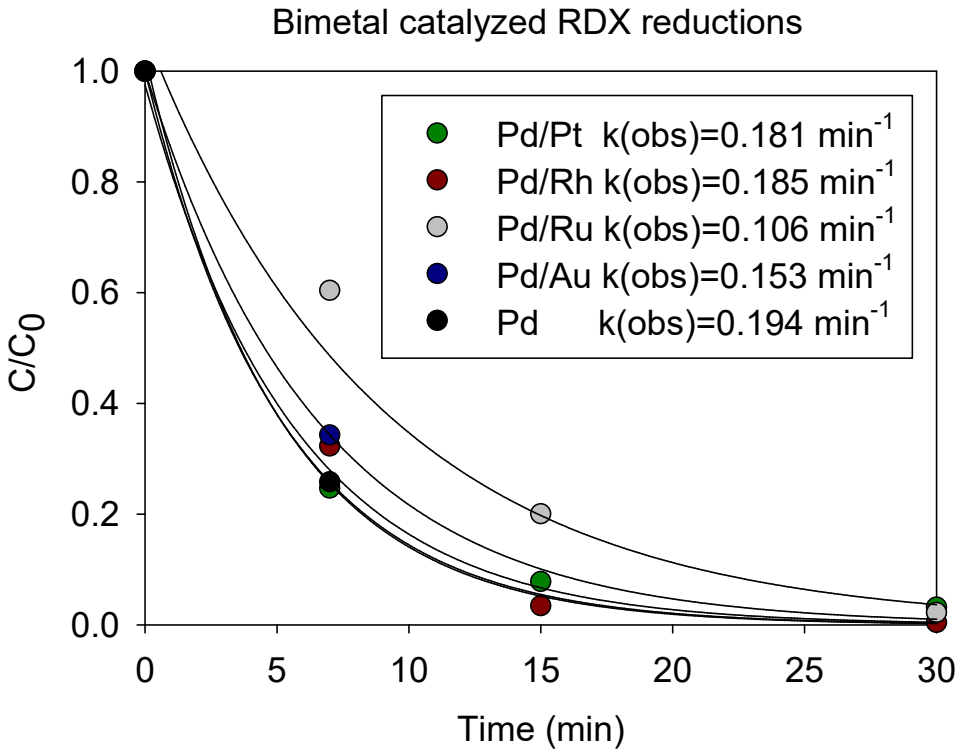

Figure 4.4. RDX Degradations in the Four Bimetallic Catalysts Reactors -- Pt-MPfR, Ru-MPfR, Rh-MPfR, and Au-MPfR -- and One Pd-film Reactor as Control.

After I computed pseudo-first-order reaction constants ($k_{(obs)}$) for all bimetallic catalysts, I normalized them by $k_{(obs)}$ for the control MPfR. The normalized results are

shown in Figure 4.5. The Pd control had the highest reactivity for RDX reduction. A secondary metal coated together with Pd could have decreased the reaction rates in two ways: (1) The bimetallic catalysts had less Pd (40 mg Pd) than with Pd alone (47.7 mg Pd), which resulted in fewer active sites for RDX reduction, if Pd provided the active sites. I will measure the actual amount of Pd coated on the membrane to support this hypothesis; (2) In addition, the secondary metal blocked the active sites on the Pd surface.

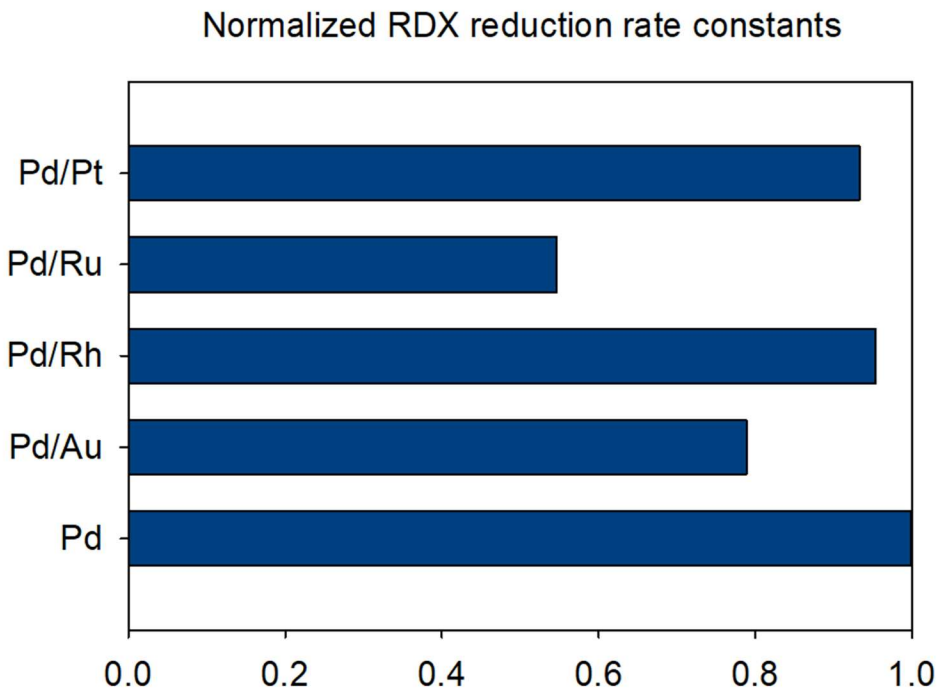

Figure 4.5. Comparison of RDX-reduction Rate Constants for the Bimetal Catalysts with Pd Alone.

4.3 Interferences Between the Energetics and the Oxyanions

To study possible interference between the energetics and the oxyanions, I conducted experiments using RDX with HMX in the MPfR and the Pd-MBfR, RDX with ClO_4^- in the Pd-MBfR, and RDX with NO_3^- in the Pd-MBfR.

Figure 4.6 presents the results of RDX and HMX reductions in the Pd-MBfR and the MPfR. Removals of RDX and HMX were more than 99% in 30 minutes for the Pd-MBfR and the MPfR. HMX had slower reduction rates than RDX in both reactors, which was consistent with the sole contaminant reductions in section 4.1. $k_{(obs)}$s were 0.073 min^{-1} and 0.074 min^{-1} for HMX in the Pd-MBfR and MPfR, respectively. The values were close to the sole contaminants reduction rates: 0.079 min^{-1} in the Pd-MBfR and 0.073 min^{-1} in the MPfRin the Pd-MBfR. The rates suggest that the presence of RDX did not harm HMX degradation. In contrast, $k_{(obs)}$ values for RDX were 0.139 min^{-1} and 0.115 min^{-1} in the presence of HMX in the Pd-MBfR and MPfR, respectively. The value was faster than the sole contaminant reductions in Pd-MBfR (0.115 min^{-1}), but slower than the sole contaminant reductions in the MPfR (0.136 min^{-1}). The possible reason is that Pd in the Pd-MBfR had higher capability that higher loading did not slow the rate; Pd in the MPfR had reached its maximum loading that mixed contaminants competed with the active sites. The higher catalysis capability in Pd-MBfR may have been attributed to the biofilm as dispersant.

Comparing RDX reductions in the Pd-MBfR and the MPfR, the MPfR had slightly higher denitration rates than the Pd-MBfR: $k_{(obs)}$ for sole RDX degradation was about 0.136 $min^{-1}$for MPfR, which was higher than 0.114 min^{-1} for Pd-MBfR. The lower

reduction rates in the Pd-MBfR probably occurred because the biofilm in the Pd-MBfR covered active sites on the Pd surface. However, the Pd-MBfR had low NO_2^- accumulation, which can be attributed to the biofilm co-working with Pd: Biofilm utilized the NO_2^- immediately after the N-N bond was broken through Pd catalytic hydrogenation.

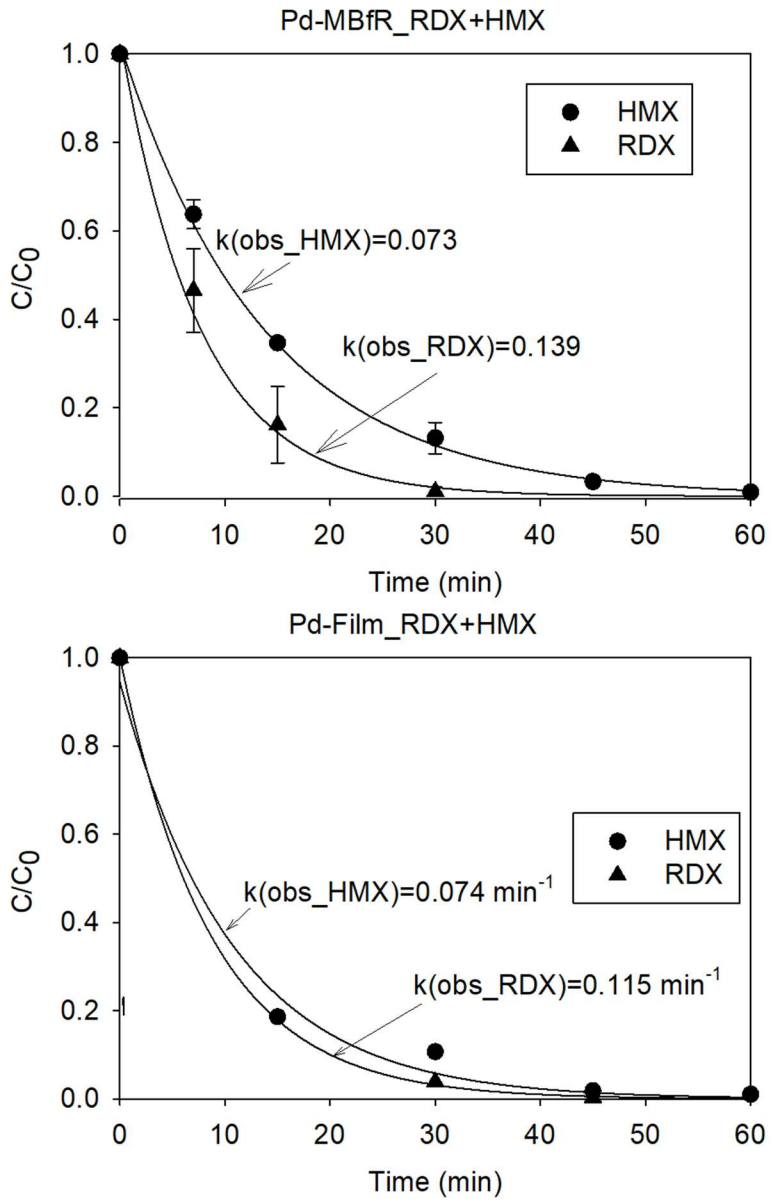

Figure 4.6. RDX and HMX Reductions in Pd-MBfR (top) and MPfR (bottom).

Tests for ClO_4^- or NO_3^- with the presence of RDX were conducted in the Pd-MBfR. The oxyanion concentrations are plotted in Figure 4.7. The results show that the presence of RDX did not harm the oxyanions reductions: $k_{(obs)}$s were 0.028 min^{-1} for NO_3^- as sole contaminant and 0.025 min^{-1} for NO_3^- with the presence of RDX; $k_{(obs)}$s were 0.0008

min^{-1} for ClO_4^- sole contaminant and 0.0011 min^{-1} for ClO_4^- with the presence of RDX. That the ClO_4^- reduction rate was higher with the presence RDX may have been caused by: (1) a more effective biofilm was present for ClO_4^- reductions in the presence of RDX; (2) the initial concentrations of ClO_4^- being lower for the test with RDX. The most important trend is that RDX did not have a large impact on reduction kinetics for NO_3^- or ClO_4^-.

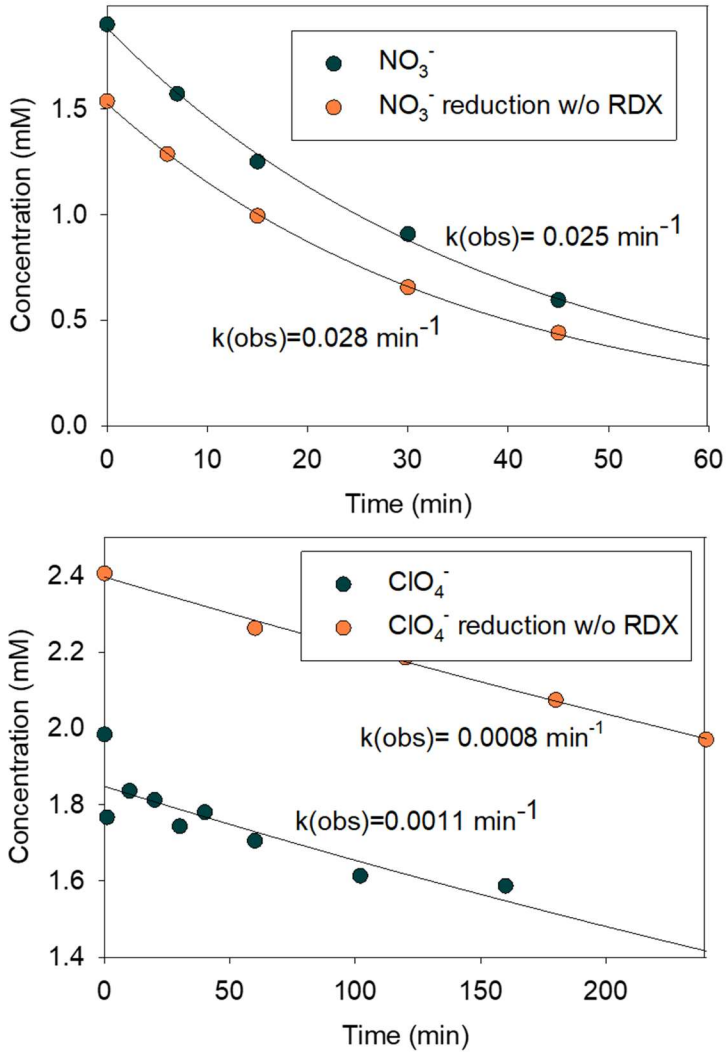

Figure 4.7. NO_3^- (top) or ClO_4^- (bottom) Reductions with the Presence of RDX in the Pd-MBfR.

Figure 4.8 summarizes the electron fluxes for all reactions. The (1) and (2) panels show that reduction of the energetics did not harm the reductions of oxyanions in the Pd-MBfR. Perhaps the electron flux values were somewhat higher with RDX present due to differences in the biofilm or the initial concentration, but the difference were minimal. The lack of inhibition by RDX suggests that NO_3^- and ClO_4^- were not reduced by the same mechanisms in the Pd-MBfR. In particular, RDX was exclusively reduced by Pd catalysis, while reductions of NO_3^- and ClO_4^- were primarily or totally biological.

The (3) and (5) panels show that HMX slowed RDX loss in the MPfR and the Pd-MBfR, although the effects were small. Likewise, the (4) and (6) panels show that RDX had minimal impact on HMX reduction. Based on the presumed nitroamine degradation reaction, denitration of 1 mol RDX with 100% selectivity to NO_2^- consumes 6 mol e^- equivalent; denitration of 1 mol HMX consumes 8 mol e^- equivalent. In the batch test of RDX with HMX in the Pd-MBfR, the average removal rates over the first 15 minutes were 3.3 meq/m^2-day for RDX and 2.5 meq/m^2-day for HMX, corresponding to 57% for RDX and 43% for HMX electron distribution. In the MPfR, similar results were observed: RDX and HMX were responsible for 52% (3.7 meq/m^2-day) and 48% (2.4 meq/m^2-day) of electron consumption, respectively. Since the distribution of electron flux for RDX and HMX were nearly even and neither had a significant inhibitory effect on the other, nitrosamine reduction probably was not near the catalytic capacity of the Pd catalyst. The RDX and HMX flux wer much less than H_2 delivery capacity (1600 meq/m^2-day), which supports that H_2 delivery was not a limitation.

In the test of RDX with NO_3^-, the average rates were 18.9 meq/m^2-day for NO_3^- and 3.1 meq/m^2-day for RDX in Pd-MBfR over the first 15 minutes; thus, NO_3^- had a 6-fold higher electron flux than RDX, which might explain the small slowdown of RDX removal in the presence of NO_3^-. However, the effect was small, probably because the H_2 delivery capacity was far in excess of the electron-consumption rate.

RDX in the presence of ClO_4^- had an increased reduction rate (0.166 min^{-1}). The average removal rates in the Pd-MBfR over the first 15 minutes were 5.0 meq/m^2-day and 2.0 meq/m^2-day for RDX and ClO_4^-, respectively. This difference may have been due to a different level of biofilm activity between the two experiments.

Comparing the reduction rates using electron fluxes, the electron fluxes were NO_3^- > RDX ~ HMX > ClO_4^-. Not taking into account the concentrations of the four oxidized compounds in the Pd-MBfR, these results suggest that the Pd-catalyzed kinetics for RDX and HMX lie intermediate between the biologically catalyzed kinetics for NO_3^- and ClO_4^-.

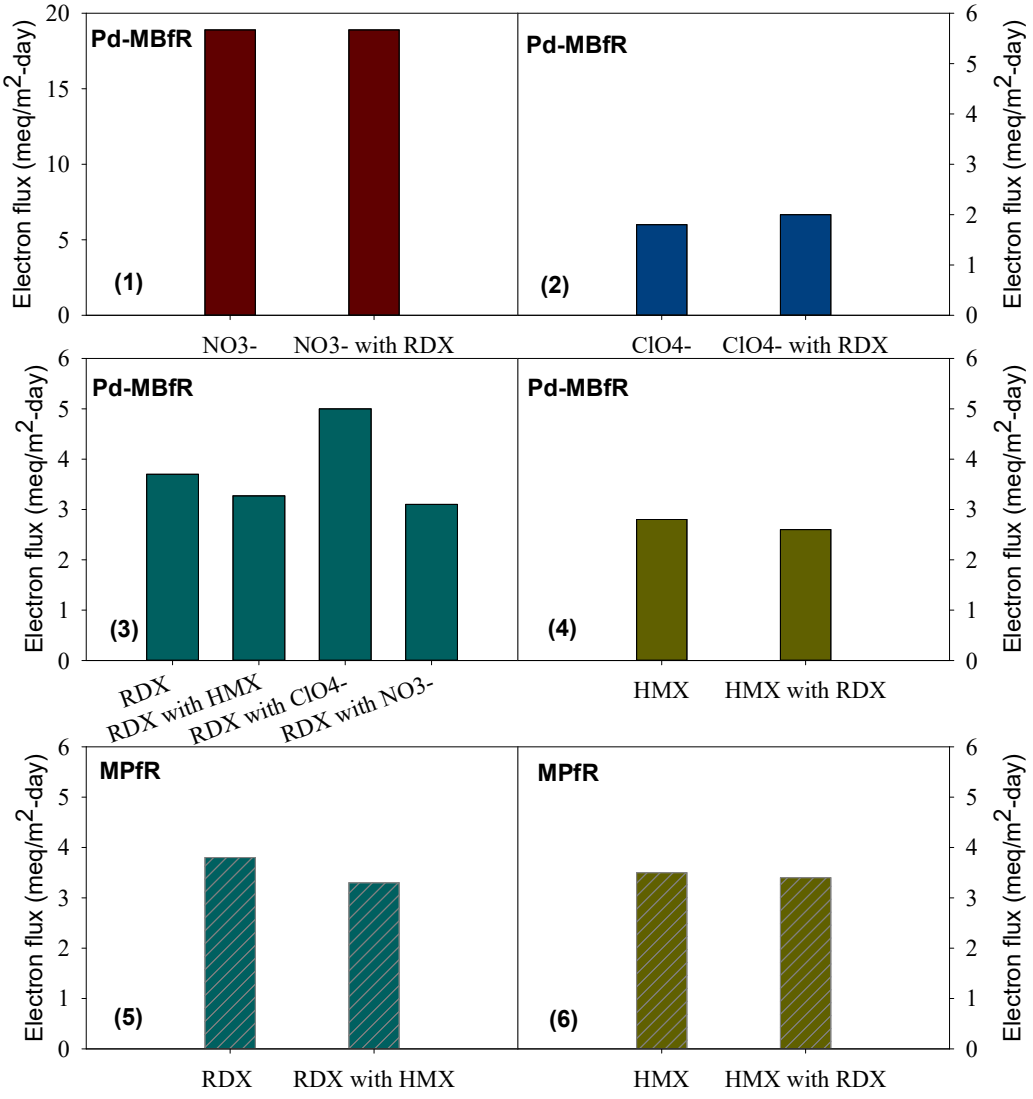

Figure 4.8. Comparison of Electron Fluxes. (1) NO_3^- reduction with or without RDX in the Pd-MBfR. (2) ClO_4^- reduction with or without RDX in the Pd-MBfR. (3) RDX reduction with or without the presence of HMX, ClO_4^-, or NO_3^- in the Pd-MBfR. (4) HMX reduction with or without RDX in the Pd-MBfR. (5) RDX reduction with or without HMX in the MPfR. (6) HMX reduction with or without RDX in the MPfR.

4.4 Degradation Pathway of RDX

The disappearance of RDX in the MPfR and Pd-MBfR was concomitant with the formation and accumulation of NO_2^-. Since conventional biological treatment is not effective in removing RDX, study on the intermediates of RDX decomposition by Pd catalysts is important.

I detected intermediates of RDX decomposition in the MPfR using atmospheric pressure ionization and high-resolution mass spectrometry (HRMS), which is illustrated in Section 2.2. When the sample solution was directly infused into the source, several signals appeared, as shown in Figure 4.9. Figures 4.9 (A) and (b) are the mass spectra of the liquid sample at the 15^{th}-minute and the 45^{th}-minute of the RDX batch test in the MPfR, respectively. The hydrogen adducts [M+H] and sodium adducts [M+Na] were detected during positive mode LC/MS-APCI.

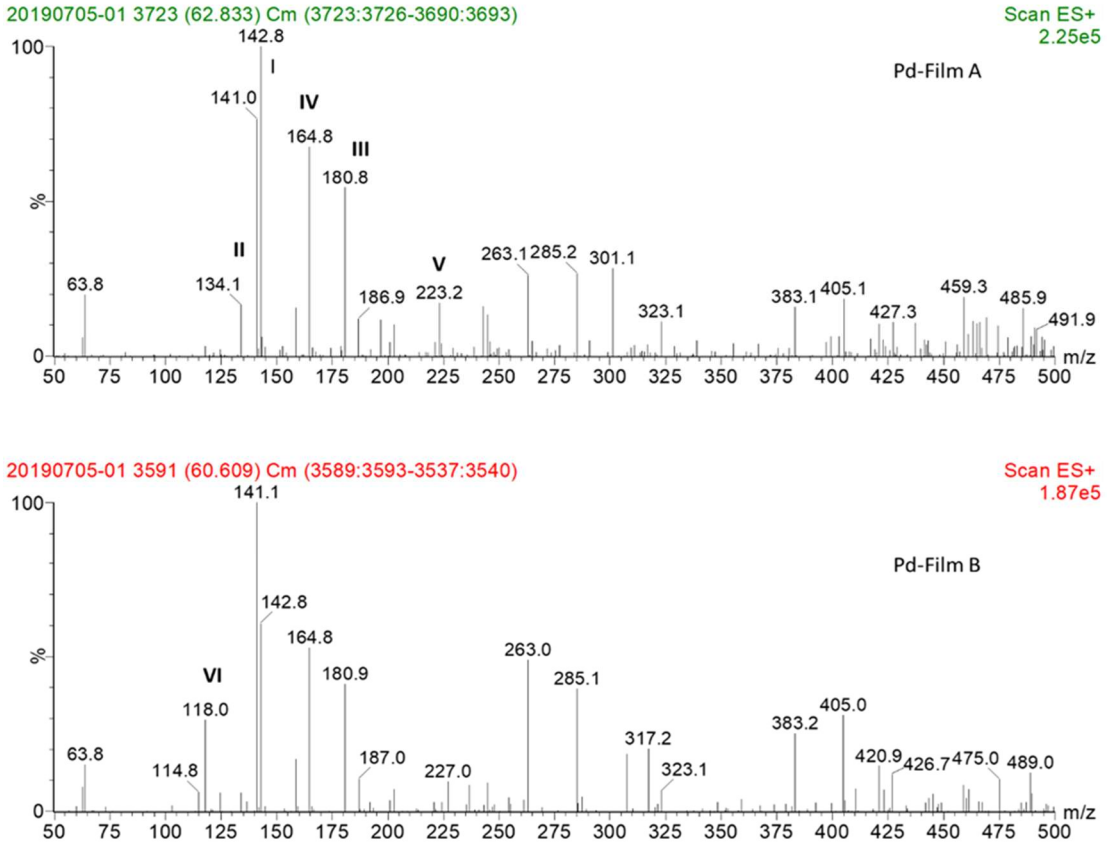

Figure 4.9. The Mass Spectra of RDX Degradation Intermediates in the Positive Mode. (A) Intermediates in MPfR at the 15th minute (top). (B) Intermediates in MPfR at the 45th minute (bottom).

The most abundant protonated molecular ions [M+H] were detected at m/z 143, 134, 181,165, 223, and 118, corresponding to the product ion I, II, III, IV, V, and VI presented in Figure 4.10. The mass data of intermediate VI matched the molecular formula of RDX. The major compound at m/z 223 corresponded to [RDX+H]. The intermediates I and II showed mass ion [M+H] at m/z 142 and 134, matching the molecular formula of high yield compounds of dinitroso-RDX (DNX). The intermediates III, IV, and V, corresponding to m/z at 181, 165, and 118, had the same characteristic fragment ions,

representing –N–NHOH. Based on these exact MS measurements, the intermediates III and V were determined to be trihydroxylamino-1,3,5-triazine and hydroxylamino-dihydro-1,3,5-triazine, respectively.

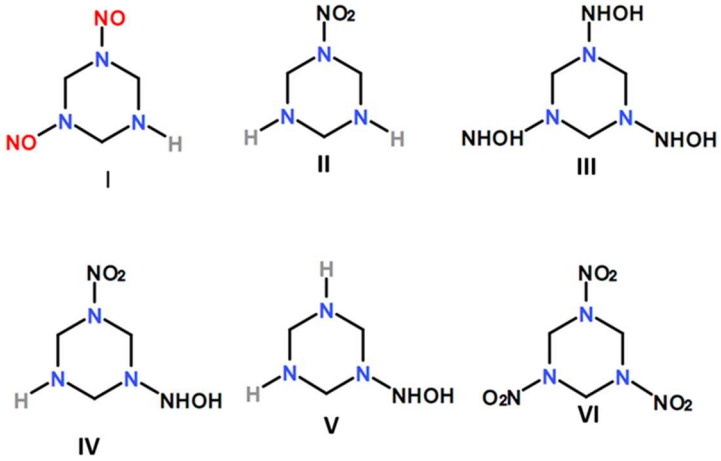

Figure 4.10. Compilation of Structures for Intermediates Identified in the Treated Wastewater by LC/MS.

Other researchers have observed hydroxylamine derivatives as RDX electrocatalytic degradation products (Y. Chen et al., 2011) and biotransformation products (Adrian & Chow, 2001). My results clearly show that these compounds were formed with my experimental conditions, and the strong intensities of the I, III, and IV in the mass spectra for hydroxylamine derivatives, amine derivatives, and nitroso derivatives indicate that they were major intermediates in the Pd-catalyzed degradation of RDX.

Based on these six exact MS measurements, I propose the degradation pathway for RDX illustrated in Figure 4.11. According to this scheme of Pd catalysis, RDX is reduced following three main reactions: (a) Pd assisted the hydroxylation of nitroso groups (N-NO) or nitro groups (N–NO_2) to hydroxylamine derivatives (N–NHOH); (b)

Pd catalyzed the sequential reduction of N–NO_2 to the corresponding N–NO groups; and (c) A N–NO_2 or N–NO linkage was catalytically cleaved to form N-H. The NO_2^- decomposed from the RDX was sequentially reduced with Pd to create N_2 or NH_4^+.

The Pd-catalyzed hydroxylation transformation means that RDX was reduced to hydroxylamine derivatives. Using Pd-based catalysts, H was formed from dihydrogen on the surface of Pd, reducing nitro groups (–NO_2) or nitroso groups (–NO) to N-hydroxylamino-N-nitrosomethylenendiamine groups (–N–NHOH). Further reactions, such as electrochemical or biological oxidation process, cleaved the derivatives and formed –N–NHOH derivatives, which were unstable and underwent hydrolysis to form nitramide and formaldehyde, decreasing the risk of chemical toxicity (A. Halasz, Spain, Paquet, Beaulieu, & Hawari, 2002; McCormick et al., 1981).

Although the high yield of III indicates that hydroxylation might be the dominant route for RDX degradation, the detection of I, II, IV, V, and NO_2^- also supports reactions b and c, which are Pd-catalyzed denitrations. Reaction b describes the sequential reduction of –NO_2 to the corresponding –NO derivatives: MNX (hexahydro-1-nitroso-3,5-dinitro-1,3,5-triazine), DNX (hexahydro-1,3-dinitroso-5-nitro-1,3,5-triazine), and TNX (hexahydro-1,3,5-trinitroso-1,3,5-triazine). This RDX degradation route was reported in RDX biodegradation under anaerobic conditions (Annamaria Halasz et al., 2012; Jian-Shen Zhao, Halasz, Paquet, Beaulieu, & Hawari, 2002). Reaction c illustrated the RDX denitrohydrogenation followed by sequential NO_2^- reduction. I detected NO_2^-, which indicates the N–NO_2 bond cleavage.

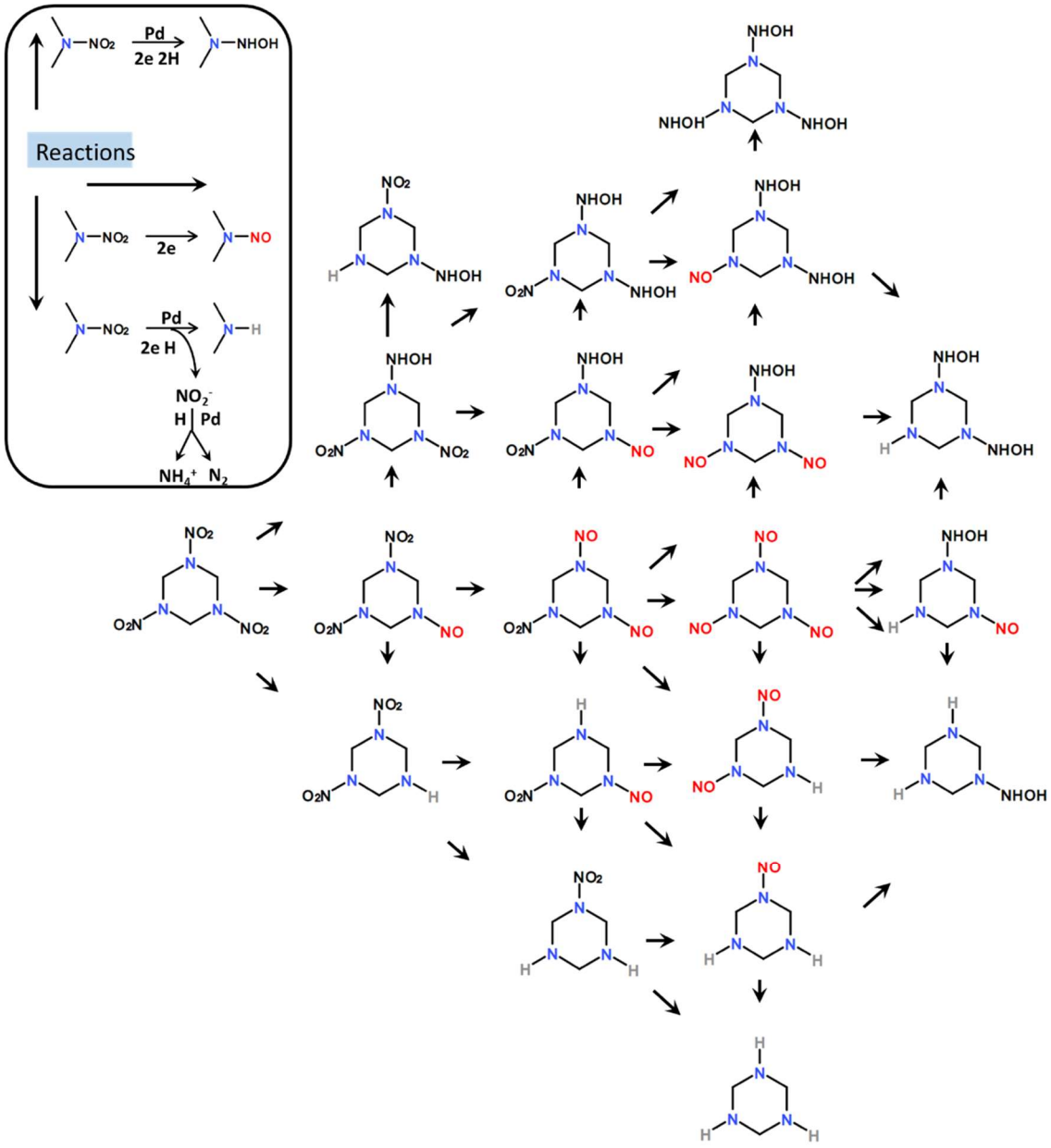

Figure 4.11. A Postulated Pd-based Transformation Pathway of RDX. The reactions in the left guided the degradation mechanisms with the corresponding directions in the right.

SUMMARY AND FUTURE WORK

Ammunition wastewater containing energetics (RDX or HMX) and oxyanions (NO_3^- and ClO_4^-) causes human-health and environmental problems without adequate treatment, which is not presently available. My study evaluated three reactors based on Pd catalysis and/or a membrane biofilm to allow H_2-based reductions. The goal is to find a highly efficient, low-cost, and sustainable means to treat energetics and oxyanions in ammunition wastewater.

Metallic catalysts were evaluated for their reduction capabilities: Pd, Rh, and Re/Pd for the oxyanions, and Pd, Pd/Pt, Pd/Ru, Pd/Rh, and Pd/Au for the energetics. Pd had the highest reactivity for NO_2^- reduction ($k_{(cat.Pd)} = 0.0004\ min^{-1}mgPd^{-1}$). Pd alone and four bimetallic catalysts — Pd/Pt, Pd/Ru, Pd/Rh, and Pd/Au — were able to reduce the two energetics. Overall, Pd showed the best potential for oxyanions and energetics reductions.

As Pd alone was not able to degrade ClO_4^- and NO_3^-, components normally present in ammunition wastewater, I coupled Pd with a biofilm to overcome Pd's limitation; this combined process is the Pd-MBfR. RDX, while recalcitrant to biodegradation in MBfR, was rapidly reduced through Pd-catalytic denitration in the Pd-MBfR (more than 99% of 90 μmol/L removed in 30 minutes in both reactors); up to 1 mmol/L ClO_4^- and 4 mmol/L NO_3^- were rapidly reduced in the Pd-MBfR. Furthermore, the oxyanions and energetics exhibited little interference between each other, and the four contaminants were degraded at the same time in the Pd-MBfR. Thus, the Pd-MBfR is an ideal means to overcome the problems of treating oxyanions and energetics together.

In the Pd-MBfR, the degradation followed three pathways that formed –N–NHOH or –N–H derivatives, which could be degraded to nitramide and formaldehyde, decreasing the risk of chemical toxicity.

The future research topics I recommend are:

1. Characterize the Pd particles on the biofilm membrane surface using Transmission Electron Microscopy (TEM).

2. Measure the exact amount of Pd coated on the membrane to normalize and compare the efficiency for different catalysts using Inductively Coupled Plasma Mass Spectrometry (ICP-MS).

3. Explore the electron competition of nitramines and oxyanions at different concentrations.

4. Explore the mechanisms of bimetallic-catalysts deactivation during ClO_3^- reduction by washing the membrane to see if the Pd reactivates.

5. Track the microbial community structure and function of the Pd-MBfR treating ammunition wastewater with energetics and oxyanions using high-throughput sequencing.

REFERENCES

Adrian, N. R., & Chow, T. (2001). Identification of hydroxylamino-dinitroso-1, 3, 5-triazine as a transient intermediate formed during the anaerobic biodegradation of hexahydro-1, 3, 5-trinitro-1, 3, 5-triazine. *Environmental Toxicology and Chemistry: An International Journal, 20*(9), 1874-1877.

Ahn, S. C., Cha, D. K., Kim, B. J., & Oh, S.-Y. (2011). Detoxification of PAX-21 ammunitions wastewater by zero-valent iron for microbial reduction of perchlorate. *Journal of hazardous materials, 192*(2), 909-914.

Ahn, S. C., Hubbard, B., Cha, D. K., & Kim, B. J. (2014). Simultaneous removal of perchlorate and energetic compounds in munitions wastewater by zero-valent iron and perchlorate-respiring bacteria. *Journal of Environmental Science and Health, Part A, 49*(5), 575-583.

Alnaizy, R., & Akgerman, A. (1999). Oxidative treatment of high explosives contaminated wastewater. *Water research, 33*(9), 2021-2030.

An, C. j., He, Y. l., Huang, G. h., & Yang, S. c. (2010). Degradation of hexahydro-1, 3, 5-trinitro-1, 3, 5-triazine (RDX) by anaerobic mesophilic granular sludge from a UASB reactor. *Journal of Chemical Technology & Biotechnology, 85*(6), 831-838.

Anotai, J., Tanvanit, P., Garcia-Segura, S., & Lu, M.-C. (2017). Electro-assisted Fenton treatment of ammunition wastewater containing nitramine explosives. *Process Safety and Environmental Protection, 109*, 429-436.

Atikovic, E., Suidan, M. T., & Maloney, S. W. (2008). Anaerobic treatment of army ammunition production wastewater containing perchlorate and RDX. *Chemosphere, 72*(11), 1643-1648.

Boopathy, R. (2001). Enhanced biodegradation of cyclotetramethylenetetranitramine (HMX) under mixed electron-acceptor condition. *Bioresource technology, 76*(3), 241-244.

Cao, T., & Li, J. (2018). *Experimental Study on the Treatment of HMX Explosive Wastewater by Fenton Process.* Paper presented at the IOP Conference Series: Earth and Environmental Science.

Caporaso, J. G., Kuczynski, J., Stombaugh, J., Bittinger, K., Bushman, F. D., Costello, E. K., . . . Gordon, J. I. (2010). QIIME allows analysis of high-throughput community sequencing data. *Nature methods, 7*(5), 335.

Caporaso, J. G., Lauber, C. L., Walters, W. A., Berg-Lyons, D., Huntley, J., Fierer, N., . . . Bauer, M. (2012). Ultra-high-throughput microbial community analysis on the Illumina HiSeq and MiSeq platforms. *The ISME journal, 6*(8), 1621.

Chaplin, B. P., Reinhard, M., Schneider, W. F., Schuth, C., Shapley, J. R., Strathmann, T. J., & Werth, C. J. (2012). Critical review of Pd-based catalytic treatment of priority contaminants in water. *Environ Sci Technol, 46*(7), 3655-3670. doi:10.1021/es204087q

Chaplin, B. P., Roundy, E., Guy, K. A., Shapley, J. R., & Werth, C. J. (2006). Effects of natural water ions and humic acid on catalytic nitrate reduction kinetics using an alumina supported Pd− Cu catalyst. *Environmental science & technology, 40*(9), 3075-3081.

Chen, X., Huo, X., Liu, J., Wang, Y., Werth, C. J., & Strathmann, T. J. (2017). Exploring beyond palladium: Catalytic reduction of aqueous oxyanion pollutants with alternative platinum group metals and new mechanistic implications. *Chemical Engineering Journal, 313*, 745-752.

Chen, Y., Hong, L., Han, W., Wang, L., Sun, X., & Li, J. (2011). Treatment of high explosive production wastewater containing RDX by combined electrocatalytic reaction and anoxic–oxic biodegradation. *Chemical Engineering Journal, 168*(3), 1256-1262.

Clark, B., & Boopathy, R. (2007). Evaluation of bioremediation methods for the treatment of soil contaminated with explosives in Louisiana Army Ammunition Plant, Minden, Louisiana. *Journal of hazardous materials, 143*(3), 643-648.

Cupples, A. M. (2013). RDX degrading microbial communities and the prediction of microorganisms responsible for RDX bioremediation. *International Biodeterioration & Biodegradation, 85*, 260-270.

Dai Lam, T., Van Chat, N., Bach, V. Q., Loi, V. D., & Van Anh, N. (2014). Simultaneous degradation of 2, 4, 6-trinitrophenyl-N-methylnitramine (Tetryl) and hexahydro-1, 3, 5-trinitro-1, 3, 5 triazine (RDX) in polluted wastewater using some advanced oxidation processes. *Journal of Industrial and Engineering Chemistry, 20*(4), 1468-1475.

DSS. (2015). *Delaware Health and Social Services Frequently Asked Qestion - HMX*.

EPA. (1985). Freshwater algae acute toxicity test.

EPA. (2014). Technical Fact Sheet – Hexahydro-1,3,5-trinitro1,3,5-triazine (RDX).

EPA. (2017). Technical Fact Sheet - Perchlorate.

Etnier, E. L. (1989). Water quality criteria for hexahydro-1, 3, 5-trinitro-1, 3, 5-triazine (RDX). *Regulatory Toxicology and Pharmacology, 9*(2), 147-157.

EwenáSmith, W. (2002). The first controlled reduction of the high explosive RDX. *Chemical Communications*(21), 2514-2515.

ExplosiVes, M. (1984). Department of the Army Technical Manual TM 9-1300-214. *Headquarters, Department of the Army: Washington, DC*, 1.

Fournier, D., Trott, S., Hawari, J., & Spain, J. (2005). Metabolism of the aliphatic nitramine 4-nitro-2, 4-diazabutanal by Methylobacterium sp. strain JS178. *Appl. Environ. Microbiol., 71*(8), 4199-4202.

Fuller, M. E., Hatzinger, P. B., Condee, C. W., & Togna, A. P. (2007). Combined treatment of perchlorate and RDX in ground water using a fluidized bed reactor. *Groundwater Monitoring & Remediation, 27*(3), 59-64.

Halasz, A., Manno, D., Perreault, N. N., Sabbadin, F., Bruce, N. C., & Hawari, J. (2012). Biodegradation of RDX nitroso products MNX and TNX by cytochrome P450 XplA. *Environmental science & technology, 46*(13), 7245-7251.

Halasz, A., Spain, J., Paquet, L., Beaulieu, C., & Hawari, J. (2002). Insights into the formation and degradation mechanisms of methylenedinitramine during the incubation of RDX with anaerobic sludge. *Environmental science & technology, 36*(4), 633-638. doi:10.1021/es011071g

Hawari, J., Beaudet, S., Halasz, A., Thiboutot, S., & Ampleman, G. (2000). Microbial degradation of explosives: biotransformation versus mineralization. *Applied microbiology and biotechnology, 54*(5), 605-618.

Hawari, J., Halasz, A., Beaudet, S., Paquet, L., Ampleman, G., & Thiboutot, S. (1999). Biotransformation of 2, 4, 6-Trinitrotoluene withPhanerochaete chrysosporium in Agitated Cultures at pH 4.5. *Appl. Environ. Microbiol., 65*(7), 2977-2986.

Hawari, J., Halasz, A., Sheremata, T., Beaudet, S., Groom, C., Paquet, L., . . . Thiboutot, S. (2000). Characterization of metabolites during biodegradation of hexahydro-1, 3, 5-trinitro-1, 3, 5-triazine (RDX) with municipal anaerobic sludge. *Appl. Environ. Microbiol., 66*(6), 2652-2657.

Heilmann, H. M., Wiesmann, U., & Stenstrom, M. K. (1996). Kinetics of the alkaline hydrolysis of high explosives RDX and HMX in aqueous solution and adsorbed to activated carbon. *Environmental science & technology, 30*(5), 1485-1492.

Hörold, S., Tacke, T., & Vorlop, K. D. (1993). Catalytical removal of nitrate and nitrite from drinking water: 1. Screening for hydrogenation catalysts and influence of reaction conditions on activity and selectivity. *Environmental Technology, 14*(10), 931-939.

Hörold, S., Vorlop, K.-D., Tacke, T., & Sell, M. (1993). Development of catalysts for a selective nitrate and nitrite removal from drinking water. *Catalysis Today, 17*(1-2), 21-30.

Hurley, K. D., & Shapley, J. R. (2007). Efficient heterogeneous catalytic reduction of perchlorate in water. *Environmental Science & Technology, 41*(6), 2044-2049.

Kitts, C. L., Cunningham, D. P., & Unkefer, P. J. (1994). Isolation of three hexahydro-1, 3, 5-trinitro-1, 3, 5-triazine-degrading species of the family Enterobacteriaceae from nitramine explosive-contaminated soil. *Appl. Environ. Microbiol., 60*(12), 4608-4611.

Kross, B., Ayebo, A., & Fuortes, L. (1992). Methemoglobinemia: nitrate toxicity in rural America. *American family physician, 46*(1), 183-188.

Li, Y., Hsieh, W.-P., Mahmudov, R., Wei, X., & Huang, C. (2013). Combined ultrasound and Fenton (US-Fenton) process for the treatment of ammunition wastewater. *Journal of hazardous materials, 244*, 403-411.

Liu, J., Choe, J. K., Wang, Y., Shapley, J. R., Werth, C. J., & Strathmann, T. J. (2014). Bioinspired Complex-Nanoparticle Hybrid Catalyst System for Aqueous Perchlorate Reduction: Rhenium Speciation and Its Influence on Catalyst Activity. *ACS Catalysis, 5*(2), 511-522. doi:10.1021/cs501286w

Liu, Z., He, Y., Li, F., & Liu, Y. (2006). Photocatalytic treatment of RDX wastewater with nano-sized titanium dioxide (5 pp). *Environmental Science and Pollution Research, 13*(5), 328-332.

Luo, Y.-H., Chen, R., Wen, L.-L., Meng, F., Zhang, Y., Lai, C.-Y., . . . Zheng, P. (2015). Complete perchlorate reduction using methane as the sole electron donor and carbon source. *Environmental science & technology, 49*(4), 2341-2349.

McCormick, N., Cornell, J. H., & Kaplan, A. (1981). Biodegradation of Hexahydro-1, 3, 5-Trinitro-1, 3, 5-Triazine. *Appl. Environ. Microbiol., 42*(5), 817-823.

Morley, M. C., Henke, J. L., & Speitel Jr, G. E. (2005). Adsorption of RDX and HMX in rapid small-scale column tests: Implications for full-scale adsorbers. *Journal of environmental engineering, 131*(1), 29-37.

Morley, M. C., Speitel, G. E., & Fatemi, M. (2006). Enhanced desorption of RDX from granular activated carbon. *Water Environment Research, 78*(3), 312-320.

Oh, S. Y., Cha, D. K., Chiu, P. C., & Kim, B. J. (2006). Zero-valent iron treatment of RDX-containing and perchlorate-containing wastewaters from an ammunition-manufacturing plant at elevated temperatures. *Water Science & Technology, 54*(10), 47. doi:10.2166/wst.2006.886

Ontiveros-Valencia, A., Tang, Y., Krajmalnik-Brown, R., & Rittmann, B. E. (2014). Managing the interactions between sulfate-and perchlorate-reducing bacteria when using hydrogen-fed biofilms to treat a groundwater with a high perchlorate concentration. *Water research, 55*, 215-224.

Panja, S., Sarkar, D., & Datta, R. (2018). Vetiver grass (Chrysopogon zizanioides) is capable of removing insensitive high explosives from munition industry wastewater. *Chemosphere, 209*, 920-927.

Parker, D. R., Seyfferth, A. L., & Reese, B. K. (2008). Perchlorate in groundwater: a synoptic survey of "pristine" sites in the coterminous United States. *Environmental science & technology, 42*(5), 1465-1471.

Pennington, J. C., & Brannon, J. M. (2002). Environmental fate of explosives. *Thermochimica Acta, 384*(1-2), 163-172.

Pouretedal, H. R., Keshavarz, M. H., Yosefi, M. H., Shokrollahi, A., & Zali, A. (2009). Photodegradation of HMX and RDX in the presence of nanocatalyst of zinc sulfide doped with copper. *Iranian Journal of Chemistry and Chemical Engineering (IJCCE), 28*(4), 13-19.

Prüsse, U., Hähnlein, M., Daum, J., & Vorlop, K.-D. (2000). Improving the catalytic nitrate reduction. *Catalysis Today, 55*(1-2), 79-90.

Prüsse, U., & Vorlop, K.-D. (2001). Supported bimetallic palladium catalysts for water-phase nitrate reduction. *Journal of Molecular Catalysis A: Chemical, 173*(1-2), 313-328.

Rahaim, R. J., & Maleczka, R. E. (2005). Pd-catalyzed silicon hydride reductions of aromatic and aliphatic nitro groups. *Organic letters, 7*(22), 5087-5090.

Ranea, V., Strathmann, T., Shapley, J., & Schneider, W. (2011). DFT Comparison of N-Nitrosodimethylamine Decomposition Pathways Over Ni and Pd. *ChemCatChem, 3*(5), 898-903.

Restivo, J., Soares, O., Órfão, J., & Pereira, M. F. R. (2015). Metal assessment for the catalytic reduction of bromate in water under hydrogen. *Chemical Engineering Journal, 263*, 119-126.

Rittmann, B. E., Nerenberg, R., Lee, K.-C., Najm, I., Gillogly, T. E., Lehman, G. E., & Adham, S. S. (2004). Hydrogen-based hollow-fiber membrane biofilm reactor (MBfR) for removing oxidized contaminants. *Water Science and Technology: Water Supply, 4*(1), 127-133.

Schaefer, C., Fuller, M., Condee, C., Lowey, J., & Hatzinger, P. (2007). Comparison of biotic and abiotic treatment approaches for co-mingled perchlorate, nitrate, and nitramine explosives in groundwater. *Journal of contaminant hydrology, 89*(3-4), 231-250.

Shin, H., Jung, S., Bae, S., Lee, W., & Kim, H. (2014). Nitrite reduction mechanism on a Pd surface. *Environmental science & technology, 48*(21), 12768-12774.

Singh, R., Soni, P., Kumar, P., Purohit, S., & Singh, A. (2009). Biodegradation of high explosive production effluent containing RDX and HMX by denitrifying bacteria. *World Journal of Microbiology and Biotechnology, 25*(2), 269-275.

Strukul, G., Gavagnin, R., Pinna, F., Modaferri, E., Perathoner, S., Centi, G., . . . Tomaselli, M. (2000). Use of palladium based catalysts in the hydrogenation of nitrates in drinking water: from powders to membranes. *Catalysis Today, 55*(1-2), 139-149.

Tang, Y., Zhou, C., Van Ginkel, S. W., Ontiveros-Valencia, A., Shin, J., & Rittmann, B. E. (2012). Hydrogen permeability of the hollow fibers used in H2-based membrane biofilm reactors. *Journal of membrane science, 407*, 176-183.

Tataurov, A. V., You, Y., & Owczarzy, R. (2008). Predicting ultraviolet spectrum of single stranded and double stranded deoxyribonucleic acids. *Biophysical chemistry, 133*(1-3), 66-70.

Terracciano, A., Ge, J., Koutsospyros, A., Meng, X., Smolinski, B., & Arienti, P. (2018). Hexahydro-1, 3, 5-trinitro-1, 3, 5-triazine (RDX) reduction by granular zero-valent iron in continuous flow reactor. *Environmental Science and Pollution Research, 25*(28), 28489-28499.

Tian, F., Hitchman, M. L., & Shamlian, S. H. (2012). Photocatalytic and photoelectrocatalytic degradation of the explosive RDX by TiO2 Thin Films Prepared by CVD and anodic oxidation of Ti. *Chemical Vapor Deposition, 18*(4-6), 112-120.

Van Aken, B., Yoon, J. M., & Schnoor, J. L. (2004). Biodegradation of nitro-substituted explosives 2, 4, 6-trinitrotoluene, hexahydro-1, 3, 5-trinitro-1, 3, 5-triazine, and octahydro-1, 3, 5, 7-tetranitro-1, 3, 5-tetrazocine by a phytosymbiotic

Methylobacterium sp. associated with poplar tissues (Populus deltoides× nigra DN34). *Appl. Environ. Microbiol., 70*(1), 508-517.

Van Ginkel, S. W., Ahn, C. H., Badruzzaman, M., Roberts, D. J., Lehman, S. G., Adham, S. S., & Rittmann, B. E. (2008). Kinetics of nitrate and perchlorate reduction in ion-exchange brine using the membrane biofilm reactor (MBfR). *Water research, 42*(15), 4197-4205.

Wataha, J., & Hanks, C. (1996). Biological effects of palladium and risk of using palladium in dental casting alloys. *Journal of oral rehabilitation, 23*(5), 309-320.

Wu, Y., Li, Y., Ontiveros-Valencia, A., Ordaz-Díaz, L., Liu, J., Zhou, C., & Rittmann, B. E. (2017). Enhancing denitrification using a novel in situ membrane biofilm reactor (isMBfR). *Water research, 119*, 234-241.

Xiong, Z., Yuan, Y., Lai, B., Yang, P., & Zhou, Y. (2016). Mineralization of ammunition wastewater by a micron-size Fe 0/O 3 process (mFe 0/O 3). *Rsc Advances, 6*(61), 55726-55735.

Ye, L., You, H., Yao, J., & Su, H. (2012). Water treatment technologies for perchlorate: a review. *Desalination, 298*, 1-12.

Zhao, H.-P., Van Ginkel, S., Tang, Y., Kang, D.-W., Rittmann, B., & Krajmalnik-Brown, R. (2011). Interactions between perchlorate and nitrate reductions in the biofilm of a hydrogen-based membrane biofilm reactor. *Environmental science & technology, 45*(23), 10155-10162.

Zhao, J.-S., Greer, C. W., Thiboutot, S., Ampleman, G., & Hawari, J. (2004). Biodegradation of the nitramine explosives hexahydro-1, 3, 5-trinitro-1, 3, 5-triazine and octahydro-1, 3, 5, 7-tetranitro-1, 3, 5, 7-tetrazocine in cold marine sediment under anaerobic and oligotrophic conditions. *Canadian journal of microbiology, 50*(2), 91-96.

Zhao, J.-S., Halasz, A., Paquet, L., Beaulieu, C., & Hawari, J. (2002). Biodegradation of hexahydro-1, 3, 5-trinitro-1, 3, 5-triazine and its mononitroso derivative hexahydro-1-nitroso-3, 5-dinitro-1, 3, 5-triazine by Klebsiella pneumoniae strain SCZ-1 isolated from an anaerobic sludge. *Appl. Environ. Microbiol., 68*(11), 5336-5341.

Zhao, J.-S., Paquet, L., Halasz, A., & Hawari, J. (2003). Metabolism of hexahydro-1, 3, 5-trinitro-1, 3, 5-triazine through initial reduction to hexahydro-1-nitroso-3, 5-dinitro-1, 3, 5-triazine followed by denitration in Clostridium bifermentans HAW-1. *Applied microbiology and biotechnology, 63*(2), 187-193.

Zhao, J.-S., Paquet, L., Halasz, A., Manno, D., & Hawari, J. (2004). Metabolism of octahydro-1, 3, 5, 7-tetranitro-1, 3, 5, 7-tetrazocine by Clostridium bifermentans strain HAW-1 and several other H2-producing fermentative anaerobic bacteria. *Fems Microbiology Letters, 237*(1), 65-72.

Zhao, J.-S., Spain, J., & Hawari, J. (2003). Phylogenetic and metabolic diversity of hexahydro-1, 3, 5-trinitro-1, 3, 5-triazine (RDX)-transforming bacteria in strictly anaerobic mixed cultures enriched on RDX as nitrogen source. *Fems Microbiology Ecology, 46*(2), 189-196.

Zhou, C., Ontiveros-Valencia, A., Wang, Z., Maldonado, J., Zhao, H.-P., Krajmalnik-Brown, R., & Rittmann, B. E. (2016). Palladium recovery in a H2-based membrane biofilm reactor: formation of Pd (0) nanoparticles through enzymatic and autocatalytic reductions. *Environmental science & technology, 50*(5), 2546-2555.

Zhou, C., Wang, Z., Ontiveros-Valencia, A., Long, M., Lai, C.-y., Zhao, H.-p., . . . Rittmann, B. E. (2017a). Coupling of Pd nanoparticles and denitrifying biofilm promotes H2-based nitrate removal with greater selectivity towards N2. *Applied Catalysis B: Environmental, 206*, 461-470.

Zhou, C., Wang, Z., Ontiveros-Valencia, A., Long, M., Lai, C.-y., Zhao, H.-p., . . . Rittmann, B. E. (2017b). Coupling of Pd nanoparticles and denitrifying biofilm promotes H 2 -based nitrate removal with greater selectivity towards N 2. *Applied Catalysis B: Environmental, 206*, 461-470. doi:10.1016/j.apcatb.2017.01.068